Thermal Conductivity of β-phase Ga₂O₃ and (AlₓGa₁₋ₓ)₂O₃ Heteroepitaxial Thin Films

Yiwen Song[1], Praneeth Ranga[2], Yingying Zhang[3], Zixuan Feng[4], Hsien-Lien Huang[5], Marco D. Santia[6], Stefan C. Badescu[6], C. Ulises Gonzalez-Valle[1], Carlos Perez[1], Kevin Ferri[7], Robert M. Lavelle[8], David W. Snyder[8], Brianna A. Klein[9], Julia Deitz[9], Albert G. Baca[9], Jon-Paul Maria[7], Bladimir Ramos-Alvarado[1], Jinwoo Hwang[5], Hongping Zhao[4,5], Xiaojia Wang[3], Sriram Krishnamoorthy[2], Brian M. Foley[1], and Sukwon Choi[1,*]

[1]Department of Mechanical Engineering, The Pennsylvania State University, University Park, Pennsylvania, 16802, USA

[2]Department of Electrical and Computer Engineering, University of Utah, Salt Lake City, Utah, 84112, USA

[3]Department of Mechanical Engineering, University of Minnesota, Minneapolis, Minnesota 55455, USA

[4]Department of Electrical and Computer Engineering, The Ohio State University, Columbus, Ohio, 43210, USA

[5]Department of Materials Science and Engineering, The Ohio State University, Columbus, Ohio, 43210, USA

[6]Materials and Manufacturing Directorate, Air Force Research Laboratory, Wright-Patterson Air Force Base, Ohio, 45433, USA

[7]Department of Materials Science and Engineering, The Pennsylvania State University, University Park, Pennsylvania, 16802, USA

[8]Electronic Materials and Devices Department, Applied Research Laboratory, University Park, Pennsylvania, 16802, USA

[9]Sandia National Laboratories, Albuquerque, New Mexico, 87185, USA

ABSTRACT: Heteroepitaxy of β-phase gallium oxide (β-Ga₂O₃) thin films on foreign substrates gives promise to the development of next-generation deep-ultraviolet (DUV) solar blind photodetectors and power electronic devices. In this work, the influences of the film thickness and crystallinity on the thermal conductivity of ($\bar{2}$01)-oriented β-Ga₂O₃ heteroepitaxial thin films were investigated. Unintentionally doped (UID) β-Ga₂O₃ thin films were grown on c-plane sapphire substrates with off-axis angles of 0° and 6° towards $< 11\bar{2}0 >$ via metalorganic vapor phase epitaxy (MOVPE) and low-pressure chemical vapor deposition (LPCVD). The surface morphology and crystal quality of the β-Ga₂O₃ thin films were characterized using scanning electron microscopy (SEM), X-ray diffraction (XRD), and Raman spectroscopy. The thermal conductivities of the β-Ga₂O₃ films were measured via time-domain thermoreflectance (TDTR). The interface quality was studied using scanning transmission electron microscopy (STEM). The measured thermal conductivities of the sub-micron thick β-Ga₂O₃ thin films were relatively low as compared to the intrinsic bulk value. The measured thin film thermal conductivities were compared with the Debye-Callaway model incorporating phononic parameters derived from first-principles calculations. The comparison suggests that the reduction in the thin film thermal conductivity can be partially attributed to the enhanced phonon-boundary scattering when the film thickness decreases. They were found to be a strong function of not only the layer thickness but also the film quality, resulting from growth on substrates with different offcut angles. Growth of β-Ga₂O₃ films on 6° offcut sapphire substrates was found to result in higher crystallinity and thermal conductivity than films grown on on-axis c-plane sapphire. However, the β-Ga₂O₃ films grown on 6° offcut sapphire exhibit a lower thermal boundary conductance at the β-Ga₂O₃/sapphire heterointerface. In addition, the thermal conductivity of MOVPE-grown ($\bar{2}$01)-oriented β-(AlₓGa₁₋ₓ)₂O₃ thin films with Al compositions ranging from 2% to 43% were characterized. Because of phonon-alloy disorder scattering, the β-(AlₓGa₁₋ₓ)₂O₃ films exhibit lower thermal conductivities (2.8-4.7 W/m·K) than the β-Ga₂O₃ thin films. The dominance of the alloy disorder scattering in β-(AlₓGa₁₋ₓ)₂O₃ is further evidenced by the weak temperature dependence of the thermal conductivity. This work provides fundamental insight into the physical interactions that govern phonon transport within heteroepitaxially grown β-phase Ga₂O₃ and (AlₓGa₁₋ₓ)₂O₃ thin films and lays the groundwork for the thermal modeling and design of β-Ga₂O₃ electronic and optoelectronic devices.

INTRODUCTION

β-phase gallium oxide (β-Ga$_2$O$_3$) is an emerging ultra-wide bandgap (UWBG) semiconductor which promises generational improvements in the performance and manufacturing cost of deep-ultraviolet (DUV) solar blind photodetectors[1] and power electronic devices[2]. The ultra-wide bandgap of β-Ga$_2$O$_3$ (E$_G$~4.8 eV[3]) renders the material to be transparent from visible to ultraviolet (UV) wavelengths. Moreover, alloying with Al$_2$O$_3$, i.e., forming a β-phase solid solution (Al$_x$Ga$_{1-x}$)$_2$O$_3$ (where x is the Al composition), allows bandgap engineering which makes the material suitable for DUV optoelectronic applications.[4] The large bandgap energy also translates into a high critical electric field of ~8 MV/cm[2], which gives promise to the development of compact power switches with kV-class breakdown voltages that are superior to wide bandgap semiconductor devices based on GaN and SiC. Another attractive attribute of β-Ga$_2$O$_3$ is that low cost substrates with high crystalline quality can be manufactured using melt-growth techniques, similar to the case of silicon wafers.[2]

Extensive efforts are being made on the heteroepitaxy of β-phase Ga$_2$O$_3$ and (Al$_x$Ga$_{1-x}$)$_2$O$_3$ films on non-native substrates to realize β-Ga$_2$O$_3$-on-sapphire DUV detectors with backside illumination capabilities and also heterojunction devices such as β-(Al$_x$Ga$_{1-x}$)$_2$O$_3$/Ga$_2$O$_3$ modulation-doped field effect transistors (MODFETs)[5]. Heteroepitaxy of β-Ga$_2$O$_3$ on high thermal conductivity substrates is also drawing significant attention as a potential solution for device overheating[6–9], stemming from the poor intrinsic thermal conductivity of bulk β-Ga$_2$O$_3$ (10.9-27 W/m·K[10,11]). Among diverse growth techniques, metalorganic vapor phase epitaxy (MOVPE) and low-pressure chemical vapor deposition (LPCVD) provide means to produce homogeneous, large-area, and optoelectronic/electronic-grade β-Ga$_2$O$_3$ and β-(Al$_x$Ga$_{1-x}$)$_2$O$_3$ epitaxial layers.

The key advantages of MOVPE growth of β-phase Ga$_2$O$_3$ and (Al$_x$Ga$_{1-x}$)$_2$O$_3$ films include the high growth rate (~10 μm/hr)[12], large growth process window[13], ability to handle large-area wafers, and low density of electronic defects[14]. N-type conductivity has been achieved for a wide range of carrier densities ($10^{16} – 10^{20}$ cm^{-3}) using Si as a dopant[15]. In addition, films with mobility values close to the theoretical limit of ~200 cm^2/Vs have been realized.[15] These are the highest mobility values reported so far for doped and undoped β-Ga$_2$O$_3$. By using N$_2$O as an oxygen precursor, the background doping in the films can be reduced to ~10^{14} cm^{-3}.[16] By reducing the acceptor densities to 2×10^{13} cm^{-3}, a record high low temperature hall mobility of 23,000 cm^2/Vs has been achieved.[17] The combination of high room temperature and low temperature mobilities confirm the high-quality of MOVPE-grown β-Ga$_2$O$_3$ thin films. In addition, significant progress has been made in the growth of (010) oriented β-(Al$_x$Ga$_{1-x}$)$_2$O$_3$[18–20]. N-type doping was realized for a wide range of Si doping for Al compositions up to x=0.33.[18,19] The Al composition can be further increased to x~0.5 by growing on (-201) and (100) bulk substrates.[21,22]

Low pressure chemical vapor deposition (LPCVD) is a scalable and low-cost film growth technique that has been demonstrated to produce high-quality β-Ga$_2$O$_3$ with a wide range of growth rates (~0.5-10 μm/h). High purity metallic gallium and oxygen are used as precursors. Argon is used as the carrier gas. Both homo- and heteroepitaxy of β-Ga$_2$O$_3$ with controllable n-type doping have been demonstrated by LPCVD.[23–26] ($\bar{2}$01)-oriented β-Ga$_2$O$_3$ films grown on c-plane sapphire substrates were shown to exhibit a relatively high dislocation density due to the large lattice mismatch.[23,24,27] However, it was demonstrated that the β-Ga$_2$O$_3$ crystalline quality and electronic transport properties can be significantly improved by growing on vicinal sapphire substrates, i.e., off-axis towards <11-20>.[23] The in-plane rotational domains were significantly suppressed via the use of off-axis sapphire substrates. Growth parameters of LPCVD β-Ga$_2$O$_3$ including growth temperature, chamber pressure, substrate preparation, and precursor flow rates have been comprehensively studied.[28,29]

Monoclinic-structured β-Ga$_2$O$_3$ exhibits a relatively low and anisotropic thermal conductivity. For example, the [010] direction shows a bulk thermal conductivity of 21.5-27.0 W/m·K, which is about two times higher than that along the [100] direction (9.5-16.3 W/m·K).[10,11,30] The thermal conductivity along the direction perpendicular to the ($\bar{2}$01) plane, which is most relevant to the current study, was reported to be 13.2-14.9 W/m·K.[10,11,30] As compared to bulk substrates, there are phonon scattering mechanisms that become prominent in thin films. First, when the thickness of a crystalline solid becomes comparable to the phonon mean free paths, incoherent phonon-boundary scattering reduces the thermal conductivity.[31,32] **Figure 1** shows the thermal conductivity accumulation function of bulk β-Ga$_2$O$_3$ in the direction perpendicular to the ($\bar{2}$01) plane, obtained from first principles calculation. The calculation results indicate the contribution of the acoustic phonon branches (that are the dominant heat carriers) to the bulk thermal conductivity; it was shown that low-frequency optical phonon modes with non-negligible group velocities would also contribution to the bulk thermal conductivity of β-Ga$_2$O$_3$.[33] Results indicate that the intrinsic mean free path of the acoustic phonons of β-Ga$_2$O$_3$ ranges from several nm to ~1 μm.[30] Therefore, β-Ga$_2$O$_3$ films with a thickness on the order of (and less than) ~1 μm would exhibit a strong film thickness dependence for their thermal conductivities. Second, the β-Ga$_2$O$_3$ films formed via heteroepitaxy typically possess higher concentrations of point and extended defects (including dislocations and rotational grains), as compared to melt-grown bulk substrates. Therefore, the thermal conductivity of heteroepitaxial β-Ga$_2$O$_3$ thin films can be considerably lower than that of a bulk substrate due to phonon-defect and phonon-grain boundary scattering effects.[31,32] The impact of Ga and O vacancies on the suppression of the thermal conductivity of β-Ga$_2$O$_3$ has been studied via first-principles density functional theory (DFT) calculation.[33] A weak doping dependence (phonon-impurity scattering) of the thermal conductivity of bulk substrates has been experimentally demonstrated.[10] To this end, experimental studies on how the crystallinity of β-Ga$_2$O$_3$ thin films (along with the film thickness) impacts the thermal conductivity have yet to be reported.
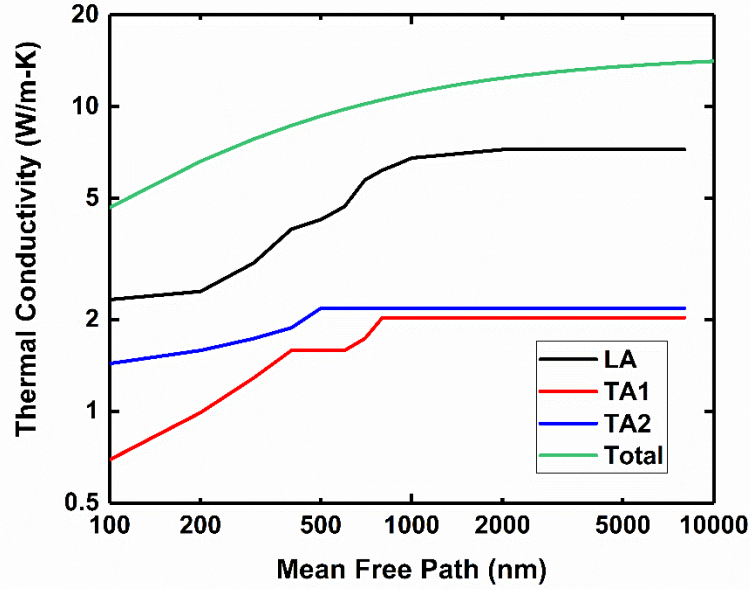
Figure 1. The thermal conductivity accumulation function for the acoustic branches of bulk β-Ga$_2$O$_3$ in the direction perpendicular to the ($\bar{2}$01) plane (at room temperature), derived from first principles calculations[30]. LA and TA are the abbreviations for longitudinal acoustic and transverse acoustic, respectively. The total thermal conductivity is obtained from the Debye-Callaway model[11]. Details can be found in the THEORETICAL CALCULATIONS section.

The film size effect on the thermal conductivity of polycrystalline Ga$_2$O$_3$ thin films grown via open atmosphere annealing of a GaN surface has been reported;[34] the measured thermal conductivities of films with a thickness range from 12.5 nm to 895 nm increased from 0.34 W/m·K to 8.85 W/m·K. Polycrystalline Ga$_2$O$_3$ thin films grown onto single crystalline diamond substrates via atomic layer deposition (ALD) were shown to exhibit a very low thermal conductivity of 1.5-1.76 W/m·K for film thicknesses range of 28-115 nm.[35] This was found to be caused by the nanocrystalline nature of the films with an average grain size of 10-20 nm. It should be noted that the materials used in the aforementioned studies lack information regarding the film orientation due to the polycrystalline nature, and do not meet requirements (e.g., electronic transport characteristics) for optoelectronic/electronic-grade materials. The film thickness dependence of the thermal conductivity of single crystalline β-Ga$_2$O$_3$ has been studied using (100)-oriented films prepared via mechanical exfoliation from a bulk substrate.[36] The thermal conductivity in the [100] direction was shown to increase from 4.7 to 11.5 W/m·K when the film thickness increased from 206 to 768 nm, approaching the bulk value of 13 W/m·K. Similarly, the thermal conductivity of a 427-nm-thick (100)-oriented β-Ga$_2$O$_3$ exfoliated film transferred onto diamond was shown to exhibit a thermal conductivity of 8.4 W/m·K, which is 35% lower than that of a bulk crystal.[37] Exfoliated films offer an opportunity to exclusively study the phonon-boundary scattering effects (i.e., the film thickness dependence of the β-Ga$_2$O$_3$ thermal conductivity), due to their high crystal quality. However, mechanical exfoliation and transfer of Ga$_2$O$_3$ are not scalable approaches for the mass production of commercial devices. Thermal transport across ($\bar{2}$01)-oriented β-Ga$_2$O$_3$ thin films heterogeneously integrated with 4H-SiC substrates via ion-cutting and surface activation bonding techniques has been demonstrated.[38] The thermal conductivity of unintentionally doped (245 nm thick; 5.35 W/m·K) and Sn-doped (255 nm thick; 2.53 W/m·K) ($\bar{2}$01)-oriented β-Ga$_2$O$_3$ epitaxial films grown on sapphire via pulsed laser deposition (PLD) has been studied.[39] PLD is a popular film growth technique in laboratory research settings because thin films with high crystal quality can be produced. However, the high cost, low throughput, and very limited area of uniform deposition are major limitations of PLD for mass production of devices. On the other hand, MOVPE and LPCVD methods offer scalable precision growth capabilities that are necessary to construct electronic and photonic devices. For this reason, MOVPE and LPCVD have attracted much attention in both fundamental and industrial perspectives. However, the resulting thermal conductivity of β-Ga$_2$O$_3$ thin films heteroepitaxially grown via MOVPE and LPCVD remain unexplored.

In addition, the thermal conductivity data of β-(Al$_x$Ga$_{1-x}$)$_2$O$_3$, which is a solid solution of monoclinic β-Ga$_2$O$_3$ and corundum α-Al$_2$O$_3$, are scarce in open literature. Only one data point at x=0.18 has been reported to date[6] while this information is critical for the electro-thermal co-design of β-Ga$_2$O$_3$ based electronic devices. For example, in a β-Ga$_2$O$_3$ modulation-doped field-effect transistor (MODFET)[5], a β-(Al$_x$Ga$_{1-x}$)$_2$O$_3$/Ga$_2$O$_3$ heterostructure is formed to create a two-dimensional electron gas (2DEG)[40] with electron mobility (potentially greater than 500 cm^2/V·s[41]) higher than that for bulk β-Ga$_2$O$_3$ (<100 cm^2/V·s^2). High-power β-Ga$_2$O$_3$ electronics are known to suffer from overheating due to the extremely high operational heat flux and the poor thermal conductivity of the base material.[6–9] Flip-chip heterointegration has been proposed to be a viable solution to overcome the intense device self-heating in β-

3

$(Al_xGa_{1-x})_2O_3/Ga_2O_3$ MODFETs.[6,7] For this device configuration, the thermal resistance associated with the β-$(Al_xGa_{1-x})_2O_3$ barrier layer must be understood to optimize the thermal design.

In this work, the cross-plane thermal conductivities of MOVPE and LPCVD grown β-phase Ga_2O_3 and $(Al_xGa_{1-x})_2O_3$ heteroepitaxial thin films have been measured using time-domain thermoreflectance (TDTR). The crystal quality of the films, resulting from growth on on-axis/off-axis c-plane sapphire substrates, was evaluated via X-ray diffraction and Raman spectroscopy. The measured data were compared with the Debye-Callaway model predictions to elucidate the fractional contributions of film thickness and the crystallinity to the reduction of the thermal conductivity of the thin films as compared to the intrinsic bulk value. Interfacial thermal transport was studied via frequency-domain thermoreflectance (FDTR) measurements and scanning transmission electron microscopy (STEM).

RESULTS AND DISCUSSION

Unintentionally doped (UID) β-Ga_2O_3 thin films with a large film thickness range of 160-4350 nm were heteroepitaxially grown on sapphire substrates with chemical and crystallographic compatibility, via LPCVD and MOVPE. Growth was performed on c-plane sapphire substrates with off-axis angles of 0° and 6° toward <11$\overline{2}$0>. This is because β-Ga_2O_3 films grown via halide vapor phase epitaxy (HVPE)[42] and LPCVD[23] on 6° off-angled c-plane sapphire substrates were shown to possess improved crystallinity, mainly because of the promotion of step flow growth and enhancement in the in-plane orientation. Details of the MOVPE and LPCVD growth procedures can be found in the EXPERIMENTAL METHODS section.

Representative top-side 50k× scanning electron microscopy (SEM) images of the MOVPE and LPCVD grown films are shown in **Figure 2**. The LPCVD films grown on sapphire substrates with 0° off-axis angle show pseudo hexagonal rotational domains (**Figure 2 (d)**). In contrast, improvement in the surface morphology is observed in the films grown on 6° off-cut substrates as evidenced by the domains aligned along the direction of the off-cut (**Figure 2 (e)**). MOVPE-grown films also show an improvement in the surface morphology; however, in a less conceivable manner (**Figure 2 (b)** and **(c)**). For comparison, SEM was also performed on a 650 μm thick commercial Fe-doped ($\overline{2}$01)-oriented bulk substrate (**Figure 2 (a)**).

Cross-sectional 20k× SEM images were taken on all samples to determine the β-Ga_2O_3 layer thickness (**Figure 2 (f)-(i)**). The average thicknesses of the β-Ga_2O_3 layers were calculated from six locations across each sample. The thickness of the Au metal transducers deposited on all samples for the TDTR measurements was measured to be 81.3±2 nm for all samples. These results were confirmed through both cross-sectional SEM and X-Ray reflectometry (XRR) analyses.

FDTR and TDTR measurements require a smooth sample surface to acquire reliable data.[31] Typically, a root-mean-square (RMS) surface roughness less than ~30 nm is necessary. The atomic force microscopy (AFM) image of a representative sample (LPCVD-grown β-Ga_2O_3 on 6° offcut sapphire; **Figure 2 (j)**) shows an RMS surface roughness of 14 nm. Only samples with an RMS surface roughness comparable to this sample, that would exhibit a similar reflected signal strength, were included in this study.
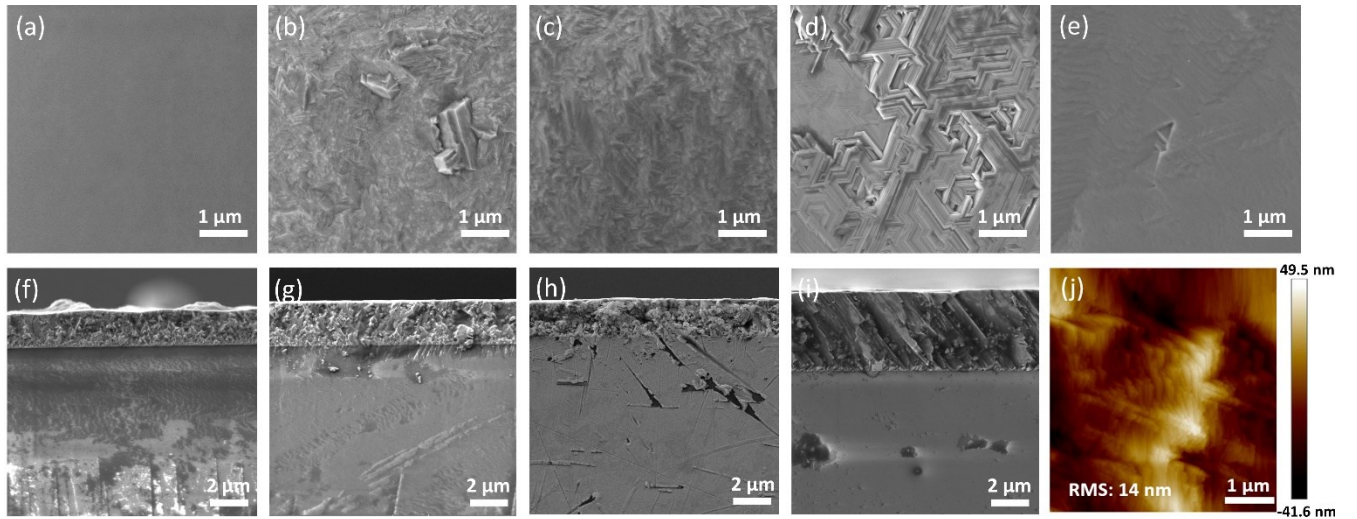

Figure 2. Representative top-view 50k× SEM images of (a) a commercial bulk substrate, MOVPE-grown films on (b) an on-axis c-plane sapphire substrate and (c) 6°off-cut sapphire substrate. LPCVD-grown films on (d) 0° and (e) 6°off-cut substrates. Also shown are cross-sectional 20k× SEM images of (f) MOVPE-grown films on 0° and (g) 6°off-cut sapphire substrates, (h) LPCVD-grown films on 0° and (i) 6°off-cut substrates. (j) AFM image and RMS surface roughness of an LPCVD-grown β-Ga_2O_3 film on a 6° offcut substrate.

X-ray diffraction (XRD) 2θ scans for the Fe-doped commercial substrate as well as the MOVPE and LPCVD-grown samples are shown in **Figure 3**. XRD 2θ scans for the bulk substrate shows the ($\bar{2}$01) orientation of the β-Ga$_2$O$_3$ material, as expected, with minor out-of-plane reflections (observable only on a logarithmic scale). The 2θ scans of the MOVPE and LPCVD-grown films reveal their ($\bar{2}$01) orientation accompanied by the (0006) sapphire substrate peak.
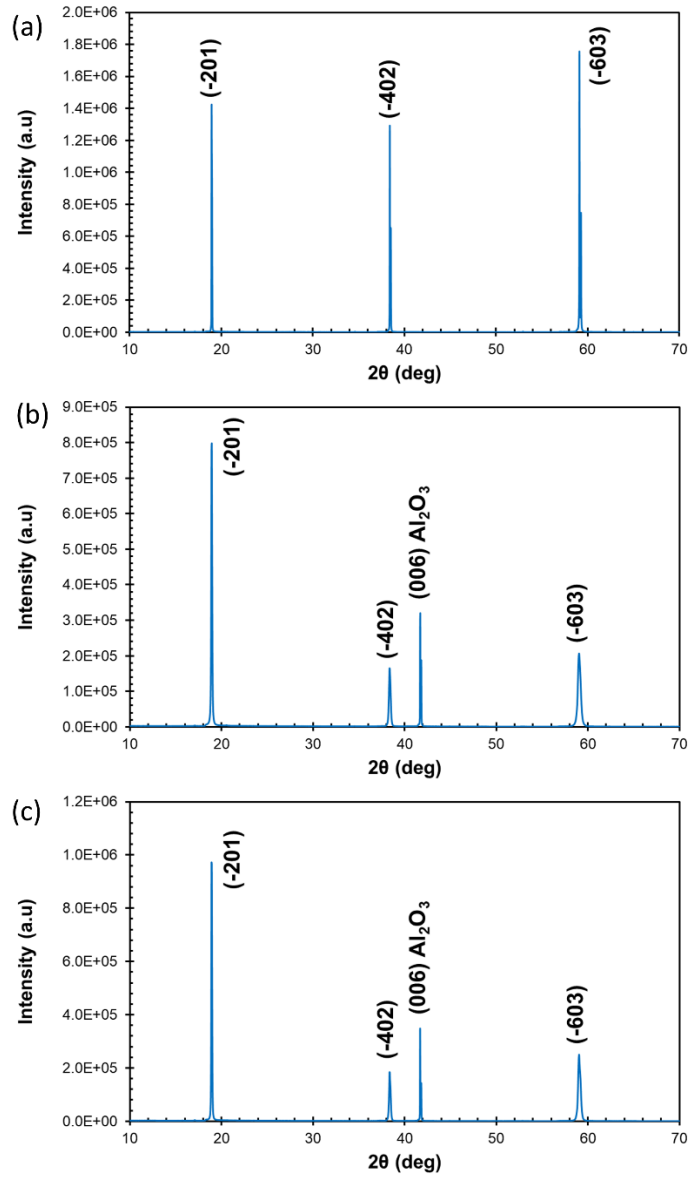
Figure 3. Representative XRD 2θ scans of (a) the ($\bar{2}$01)-orientated β-Ga$_2$O$_3$ substrate, (b) a MOVPE-grown film on a sapphire substrate, and (c) a LPCVD-grown film on a sapphire substrate.

In addition to determining the phase and orientation, the crystalline quality of the β-Ga$_2$O$_3$ films was evaluated by XRD rocking curve measurements. **Figure 4** shows the XRD rocking curves of symmetric ($\bar{4}$02) reflection peaks of the β-Ga$_2$O$_3$ films and the bulk substrate. The XRD rocking curve ω scan of the commercial substrate (**Figure 4 (a)**) shows a sharp narrow peak with a full-width-at-half-maximum (FWHM) of 0.018° (64.8 arcsec). The FWHM of the XRD rocking curves of the films grown on 6° off-cut substrates (while being significantly broader than the FWHM of the bulk β-Ga$_2$O$_3$) consistently exhibited lower values than those grown on 0° off-cut substrates, which could indicate lower screw and edge dislocation density.[43,44]
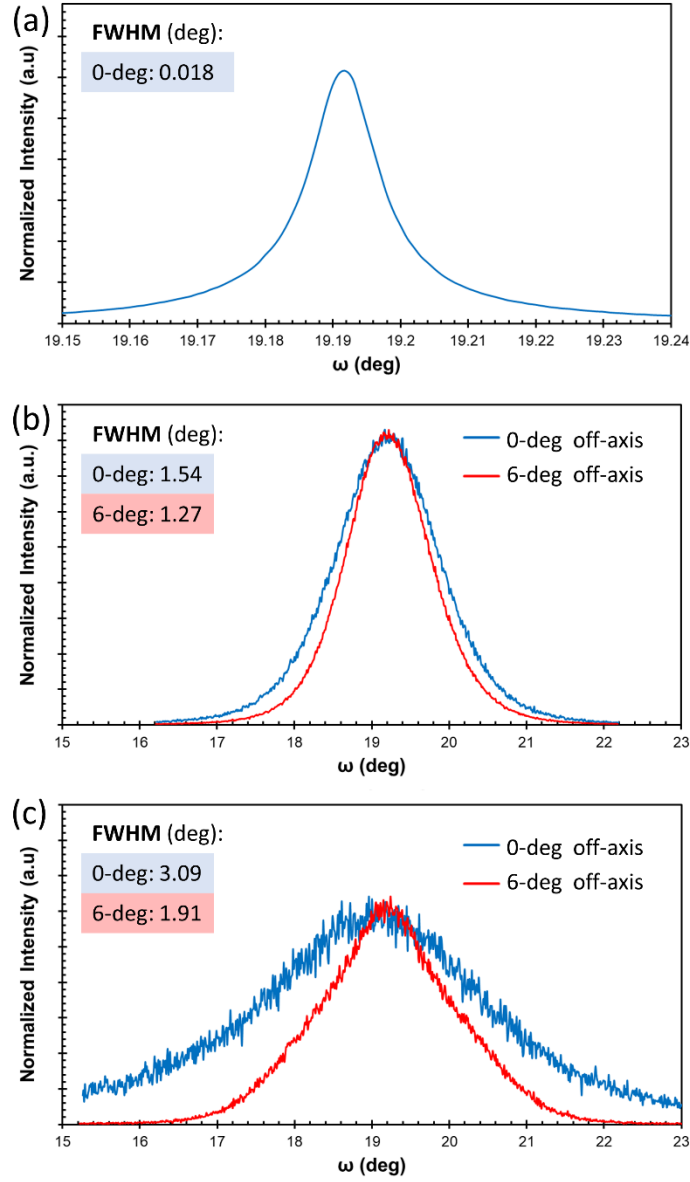
Figure 4. Representative XRD rocking curves, i.e., the symmetric ($\bar{4}$02) reflection peaks of (a) the (-201) oriented β-Ga$_2$O$_3$ bulk substrate, (b) on-axis vs. 6°off-axis MOVPE grown films, and (c) on-axis vs. 6°off-axis LPCVD grown films.

Additional qualitative assessment of the crystal quality of the films was made by performing Raman spectroscopy measurements. To assess the crystalline quality of the β-Ga$_2$O$_3$ thin films, the FWHM of the A$_g^{(3)}$ Raman peak[45] near 199.7 cm^{-1} was analyzed and also compared to the linewidth of the A$_g^{(3)}$ peak of the bulk substrate (**Figure. 5 (a)**). According to the energy-time uncertainty relation, as the crystalline quality increases, the linewidth of the phonon mode will decrease because the phonon lifetime increases.[46] For the Fe-doped bulk sample, an average FWHM of 1.62 cm^{-1} was calculated. As shown in **Figure 5 (b)**, The MOVPE 6° off-axis samples exhibited narrower FWHM values than on-axis grown samples, suggesting superior crystalline quality. Similar observations were found in the LPCVD-grown films, i.e., the 6° off-axis grown films would exhibit narrower A$_g^{(3)}$ Raman peaks, as compared to the on-axis grown films, indicating better crystallinity **(Figure 5 (c))**. The Raman measurement results are consistent with the FWHM analysis performed via XRD rocking curve measurements.
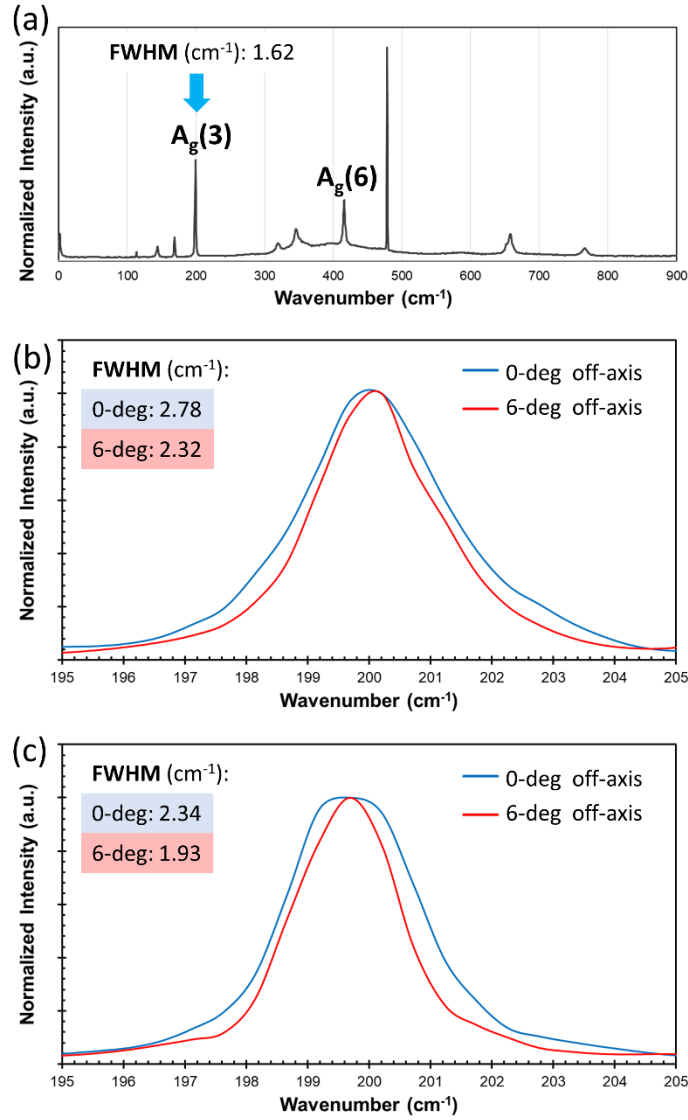
Figure 5. (a) Raman spectrum of the $(\bar{2}01)$-orientated β-Ga$_2$O$_3$ substrate. (b) Representative FWHM comparison of the Raman A$_g^{(3)}$ mode for on-axis vs. 6°off-axis MOVPE grown films. (c) A similar comparison for representative LPCVD grown films.

Cross-plane thermal conductivity measurements of $(\bar{2}01)$-orientated MOVPE and LPCVD grown β-Ga$_2$O$_3$ films, with a thickness range of 164 – 4,350 nm, were performed using time-domain thermoreflectance (TDTR)[47]. Half of the samples were grown on off-axis c-plane sapphire substrates and the rest were grown on sapphire substrates with an off-axis angle of 6° toward <11$\bar{2}$0>, as labeled in **Figure 6**. For this thickness range, TDTR measurement results show a noticeable thickness dependence of the thermal conductivity of the β-Ga$_2$O$_3$ films; specifically, the thermal conductivity reaches the bulk value for a film thickness of 4,350 nm and monotonically reduces with decreasing the thickness. The measurement results in **Figure 6** indicate that phonons with mean free paths on the order of ~1 μm carry a significant fraction of the heat in this crystalline system, which is consistent with first principles calculation results shown in **Figure 1**. As the thickness of the films drops below ~1 μm, these phonons begin to scatter at the boundaries[31,32], leading to a continuing reduction in the thermal conductivity as the thickness decreases further. Cheng et al.[38] has reported the thermal conductivity of $(\bar{2}01)$-orientated thin films prepared via ion-cutting, and the data for high temperature annealed films relieved from the implantation-induced strain are included in **Figure 6**. Likewise, a strong film thickness dependence of the thermal conductivity of β-Ga$_2$O$_3$ at room temperature for the [100] direction has been reported in literature.[36,37]

The film thickness is a main design parameter to achieve the desired thermal performance of β-Ga$_2$O$_3$ electronic devices integrated with high thermal conductivity substrates.[6,7] Therefore, the results in **Figure 6** suggest that device engineers should account for the film thickness effect on the thermal conductivity of β-Ga$_2$O$_3$ when creating device thermal models to be used for design optimization. **Figure 6** also plots the thin film thermal conductivities of β-Ga$_2$O$_3$ obtained from Debye-Callaway model predictions (dashed lines).

Based on the Debye-Callaway model, the phonon-boundary scattering rate is dominant over impurity and Umklapp scattering rates, leading to the increasing trend of thermal conductivity versus film thickness. As can be seen from **Figure 6**, both model predictions and measurement data capture the overall increasing trend of the thin film thermal conductivity when the film thickness increases; however, the predicted values are higher than those obtained from measurements for films with thicknesses ranging from 180 to 2500 nm. The discrepancies can be attributed to the crystallinity quality of the epitaxial films, which is not comparable to that of pure single crystals as assumed in the model predictions. The size effect of the β-Ga$_2$O$_3$ thermal conductivity is more notable for (100)-oriented films exfoliated from a single crystal β-Ga$_2$O$_3$ wafer due to the consistency in the crystalline quality of the films.[36]

The β-Ga$_2$O$_3$ films MOVPE-grown over 6° off-axis substrates exhibit a 10-30% higher thermal conductivity as compared to the films grown on on-axis c-plane sapphire substrates with comparable thickness. This aligns with the SEM, XRD, and Raman characterization results, showing improvement in the surface morphology and crystal quality for films grown on sapphire substrates with a 6° off-cut angle for both MOVPE and LPCVD-grown β-Ga$_2$O$_3$ thin films. It should be noted that the atomic steps provided by the off-cut substrates regulate the nucleation of the growth, which improves the crystalline quality. In other words, the off-cut surface steps terminate the interface defects more effectively.
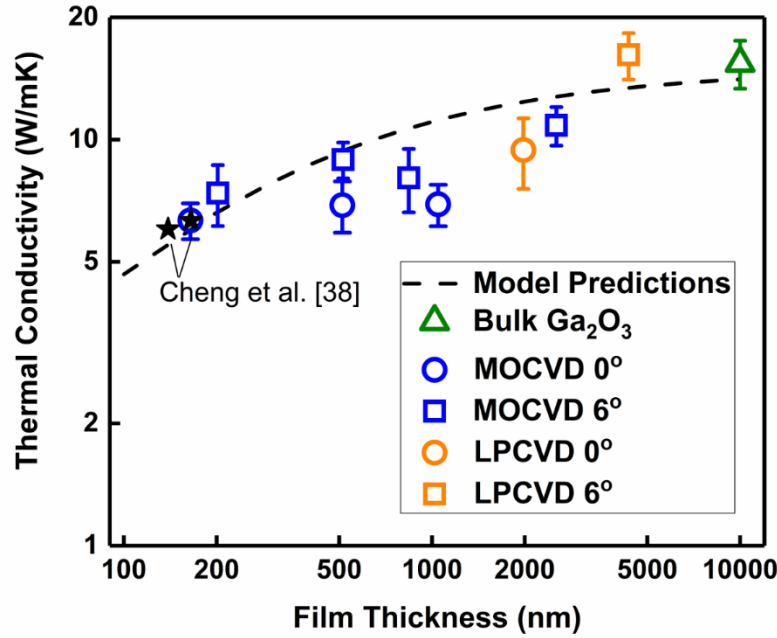

Figure 6. The measured cross-plane thermal conductivities of the ($\bar{2}$01)-orientated β-Ga$_2$O$_3$ thin films and the bulk substrate. Predictive modeling results that estimate the thickness dependence of the β-Ga$_2$O$_3$ thermal conductivity in a direction perpendicular to the ($\bar{2}$01) plane are shown for comparison. Also shown are two data points for ($\bar{2}$01)-orientated thin films prepared via ion-cutting from Cheng et al.[38]

Heteroepitaxy of β-Ga$_2$O$_3$ on high thermal conductivity substrates is a potential thermal management solution for β-Ga$_2$O$_3$ based devices; therefore, understanding thermal transport across the β-Ga$_2$O$_3$/substrate interface is important. Frequency-domain thermoreflectance (FDTR)[48] was used to measure the thermal boundary conductance (TBC) at the β-Ga$_2$O$_3$/sapphire interface of the heteroepitaxial films. The interface TBC measurements were performed on a 164 nm thick MOVPE-grown β-Ga$_2$O$_3$ film on c-plane sapphire and a 202 nm thick MOVPE-grown β-Ga$_2$O$_3$ layer on off-cut sapphire. These samples offered higher measurement sensitivity to the TBC as compared to the thicker films. FDTR was used for TBC measurement because TDTR would not offer sufficient measurement sensitivity to this parameter due to the shallower probing depth, owing to the higher pump modulation frequency. The cross-plane thermal conductivity of the films was treated as a known parameter based on the TDTR measurement results listed in Figure 6. For comparison, the TBC at the ($\bar{2}$01) β-Ga$_2$O$_3$/sapphire substrate interfaces were calculated using the acoustic mismatch model (AMM) and diffusive mismatch model (DMM). The AMM and DMM$_1$ were calculated following the implementation presented by Bellis et al.[49] As shown in Figure 7, the β-Ga$_2$O$_3$ grown on the c-plane sapphire substrate has a higher TBC than the β-Ga$_2$O$_3$ grown on the sapphire substrate with an off-axis angle. It is important to note that even for the thinnest film (164 nm thick), FDTR does not offer high enough measurement sensitivity to quantify the TBC with low uncertainty. Nevertheless, the results still provide a qualitative assessment of the relative magnitude of the TBCs associated with the heterointerfaces of β-Ga$_2$O$_3$ films grown on c-plane and offcut sapphire substrates. The upper range of the TBC for the β-Ga$_2$O$_3$ film grown on c-plane sapphire is difficult to

determine because FDTR loses sensitivity to the TBC when its value is high; therefore, its upper bound was chosen to be the AMM predicted value. Also shown in Figure 7 is the DMM result calculated by Cheng et al.[38] for the TBC between ($\bar{2}$01) β-Ga$_2$O$_3$ and c-plane sapphire (listed as DMM$_2$). Their model is based on the Landauer formula accounting for temperature-dependent phonon properties. The measured TBC results indicate that while growing β-Ga$_2$O$_3$ on a substrate with an offcut angle improves the crystalline quality due to the promoted step flow growth,[23] the interfacial phonon transport is restricted as compared to films grown on on-axis c-plane sapphire.
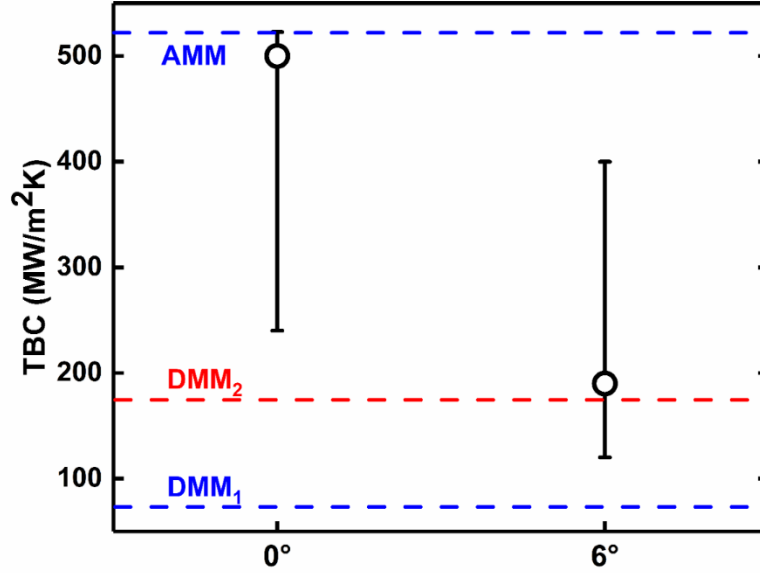

Figure 7. The measured thermal boundary conductance of β-Ga$_2$O$_3$ grown on 0° and 6° off-axis c-plane sapphire substrates (open circles with error bars). Due to the lack of sensitivity, the upper limit for the 6° sample cannot be experimentally determined; therefore, it is artificially bounded by the AMM predictions. The AMM and DMM$_1$ are calculated following the methodology presented by Bellis et al.[49] The DMM$_2$ was adopted from Cheng et al.[38]

The structural quality of the film interfaces between the β-Ga$_2$O$_3$ and both the on-axis and 6° off-axis substrates were investigated using cross-sectional scanning transmission electron microscopy (STEM) imaging. The representative images from both samples are shown in **Figure 8**. The images indicate that the interface of the on-axis grown sample (**Figure 8 (a)**) shows a smooth interface with a low density of structural defects. On the other hand, the 6° off-axis grown sample (**Figure 8(b)**) shows a relatively higher degree of defects at the interface with more structural distortion and apparent strain field around the defective regions. The defective interface likely impedes the heat flow, which leads to the lower TBC measured from the 6° off-axis grown samples (**Figure 7**).
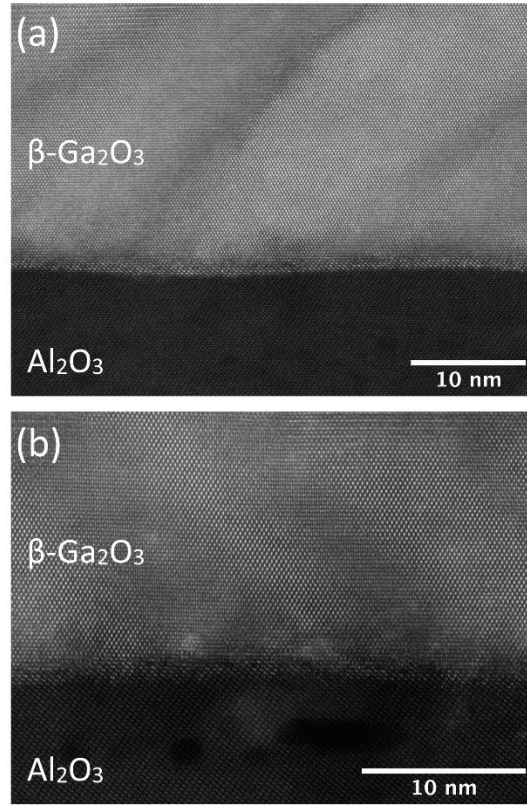
Figure 8. Atomic scale STEM images representing β-Ga$_2$O$_3$ films grown on (a) 0° and (b) 6° off-axis c-plane sapphire substrates.

TDTR measurements were performed on MOVPE-grown ($\bar{2}$01)-oriented β-(Al$_x$Ga$_{1-x}$)$_2$O$_3$ films with various Al compositions (x = 0.08 – 0.43). The thickness of the films ranged 184 – 752 nm, where the films with lower x were thicker. For example, the thicknesses of the x=0.08, 0.27, and 0.43 films were 752 nm, 505 nm, and 184 nm, respectively. The measured cross-plane thermal conductivities for films with different Al compositions (x) are summarized in **Figure 9**. The thermal conductivity of the β-(Al$_x$Ga$_{1-x}$)$_2$O$_3$ films ranged 2.8 – 5.6 W/m·K, which is ~50% lower than those for β-Ga$_2$O$_3$ films of similar thickness. This large discrepancy between the thermal conductivity of β-Ga$_2$O$_3$ and β-(Al$_x$Ga$_{1-x}$)$_2$O$_3$ films is mainly attributed to phonon-alloy disorder scattering[50], which is known to severely restrict the mean free path of phonons. Similarly, the thermal conductivity of Al$_x$Ga$_{1-x}$N was reported to be an order of magnitude lower than those for the constituent base crystals, GaN and AlN.[51] While the β-Ga$_2$O$_3$ films exhibited a strong thickness dependence of their thermal conductivities, the β-(Al$_x$Ga$_{1-x}$)$_2$O$_3$ thermal conductivity values are relatively invariant with respect to the film thickness. This may indicate vibrational modes with considerably shorter mean free paths than β-Ga$_2$O$_3$ dominate thermal transport within the alloy.[52] On the other hand, the β-(Al$_x$Ga$_{1-x}$)$_2$O$_3$ films that were grown on 6° off-axis substrates still exhibit a higher thermal conductivity than films grown on on-axis sapphire substrates. Despite phonon scattering caused by compositional disorder dominates the thermal conductivity of β-(Al$_x$Ga$_{1-x}$)$_2$O$_3$, phonon scattering with point/extended defects and rotational grain boundaries still impacts the overall thermal transport within the solid solution.
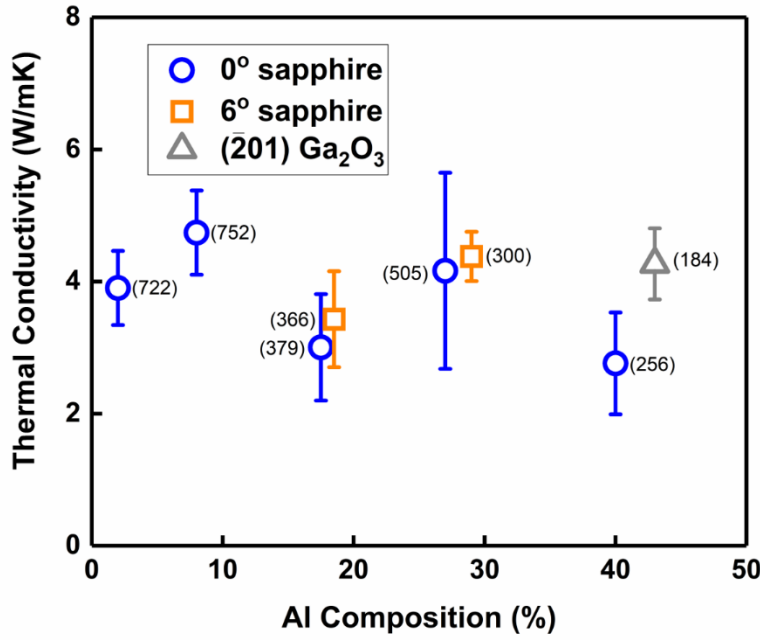
Figure 9. The compositional dependence of the thermal conductivity of β-(Al$_x$Ga$_{1-x}$)$_2$O$_3$ thin films. The numbers in the parentheses are the corresponding β-(Al$_x$Ga$_{1-x}$)$_2$O$_3$ film thicknesses in nanometers. The 366 nm and the 379 nm films have identical Al compositions of 18%; however, their Al compositions have been offset for an illustrative purpose.

Temperature-dependent thermal conductivity measurements were performed on β-Ga$_2$O$_3$ (521 nm) and β-(Al$_{0.27}$Ga$_{0.73}$)$_2$O$_3$ (505 nm) films with a similar thickness using TDTR from room temperature up to 600 ˚C (**Figure 10**). As the temperature increases, the thermal conductivity of the β-Ga$_2$O$_3$ film monotonically decreases due to the increased Umklapp scattering rate; the temperature-dependent thermal conductivity of bulk β-Ga$_2$O$_3$ shows a similar trend and has been reported in literature[53]. In contrast, the thermal conductivity of the β-(Al$_{0.27}$Ga$_{0.73}$)$_2$O$_3$ film is relatively invariant across this temperature range. A similar trend was previously observed in solid solutions Al$_{1-x}$Ga$_x$N[51] and Al$_x$Sc$_{1-x}$N[54]. The tested temperature range reaches up to the Debye temperatures of the two constitutive materials (α-Al$_2$O$_3$[55] and β-Ga$_2$O$_3$[56]). The relatively constant thermal conductivity of β-(Al$_x$Ga$_{1-x}$)$_2$O$_3$ within this temperature range suggests that phonon-phonon scattering is not the dominating scattering mechanism, in contrast to the case of β-Ga$_2$O$_3$. Instead, phonon-alloy disorder scattering dominates the thermal conductivity of the β-(Al$_x$Ga$_{1-x}$)$_2$O$_3$ solid solution. It is interesting to note that the temperature-dependent thermal conductivity of β-(Al$_x$Ga$_{1-x}$)$_2$O$_3$/Ga$_2$O$_3$ superlattices has also been reported[53]; the thermal conductivity increases with temperature up to 380K, due to phonon-structural imperfection scattering effects associated with the large number of boundaries. It is imperative to understand the dominant phonon scattering mechanisms associated with different β-Ga$_2$O$_3$ and β-(Al$_x$Ga$_{1-x}$)$_2$O$_3$ material platforms to understand the self-heating behavior of devices based on them.
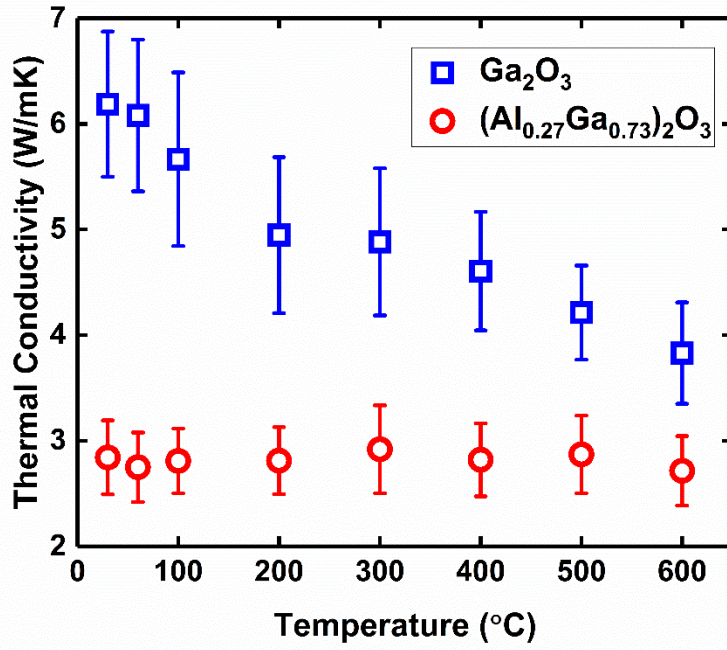
Figure 10. The temperature dependence of the thermal conductivity of ~500 nm thick β-Ga₂O₃ and β-(AlₓGa₁₋ₓ)₂O₃ thin films.

Raman spectroscopy measurements were performed on the β-(AlₓGa₁₋ₓ)₂O₃ films as a function of Al composition. **Figure 11** presents the Raman spectra of β-(AlₓGa₁₋ₓ)₂O₃ films grown on sapphire, and the Raman spectrum of a bare sapphire substrate. Raman peaks of the Ga₂O₃ (x = 0) film are marked in **Figure 11**. The incorporation of Al atoms causes a blueshift in the Raman peak positions and reduces the peak intensity. At x = 0.40, the $A_g^{(3)}$ peak flattens and cannot be identified. The peak position (P [cm⁻¹]) of the $A_g^{(3)}$ Raman peak can be roughly correlated to the Al composition (x) up to 27% as $P[cm^{-1}] = 201.382 + 0.107\,x$; however, it should be noted that not only the Al composition but also the strain in the films will influence the Raman peak position.
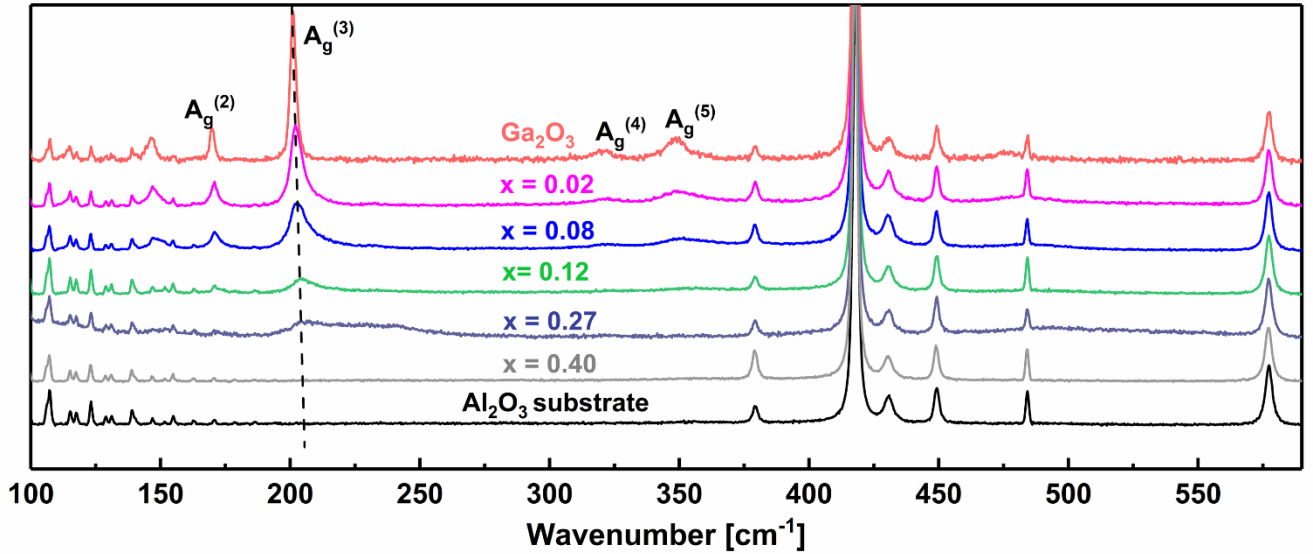
Figure 11. Raman spectra of the β-(AlₓGa₁₋ₓ)₂O₃ films as a function of Al composition (x) and the Raman spectrum of the sapphire substrate. The dashed line qualitatively shows the blueshift of the $A_g^{(3)}$ mode as x increases.

12

CONCLUSIONS

Heteroepitaxial growth of β-Ga$_2$O$_3$ via LPCVD and MOVPE has significant technological importance in terms of the mass production of optoelectronic/electronic-grade β-Ga$_2$O$_3$ and β-(Al$_x$Ga$_{1-x}$)$_2$O$_3$ thin films. This work investigated physical mechanisms that govern the thermal transport across β-Ga$_2$O$_3$ and β-(Al$_x$Ga$_{1-x}$)$_2$O$_3$ thin films grown on foreign substrates. First, a strong thickness dependence of the thermal conductivity was observed in β-Ga$_2$O$_3$ films with submicrometer thickness. The thermal conductivity would monotonically increase with the thickness where-in a 4,350 nm-thick film would exhibit the bulk thermal conductivity. This thickness dependence was confirmed by a Debye-Callaway model, which indicates that phonon-boundary scattering is dominant over other scattering mechanisms (at room temperature), leading to the observed thickness-dependent thermal conductivity. Second, the crystallinity of the samples impacts thermal transport within the β-Ga$_2$O$_3$ films. The β-Ga$_2$O$_3$ films grown on 6° off-axis sapphire substrates exhibited a 10 – 30% higher thermal conductivity as compared to films grown on on-axis c-plane sapphire substrates with a comparable thickness. The higher thermal conductivity of films grown on offcut substrates is attributed to the higher crystalline quality of the films, confirmed by SEM, XRD, and Raman measurements. The interface quality of the films grown on the 0° and 6° off-axis sapphire substrates was evaluated using atomic scale STEM imaging. Data reveals that the interface quality of the samples grown on 6° off-axis substrates is inferior to the on-axis grown samples, which leads to a higher TBC. In addition, the thermal conductivity of MOVPE-grown β-(Al$_x$Ga$_{1-x}$)$_2$O$_3$ films with various Al compositions (x = 0.08 – 0.43) was measured. A significant reduction (>50%) in the thermal conductivity was observed for the β-(Al$_x$Ga$_{1-x}$)$_2$O$_3$ films as compared to β-Ga$_2$O$_3$ films with similar thicknesses. This reduction is attributed to phonon-alloy disorder scattering, which also results in weak film thickness and temperature dependences of the β-(Al$_x$Ga$_{1-x}$)$_2$O$_3$ thermal conductivity. β-(Al$_x$Ga$_{1-x}$)$_2$O$_3$ films grown on 6° off-axis sapphire substrates exhibit higher thermal conductivities than the films grown on on-axis sapphire substrates, showing that the crystallinity still impacts thermal transport within the solid solution.

The outcomes of this study highlight the key thermal design considerations for DUV optoelectronic and power electronics applications based on heteroepitaxial β-phase Ga$_2$O$_3$ and (Al$_x$Ga$_{1-x}$)$_2$O$_3$ thin films. From a thermal engineering standpoint, the thickness of the epitaxial layers should be carefully chosen to minimize the overall device thermal resistance. From the material growth perspective, heteroepitaxy on foreign substrates with an offcut angle could improve the crystalline quality, which in turn improves the thermal and electrical performance. However, growing films on substrates with an offcut angle was shown to limit the interfacial thermal transport due to the formation of structural defects and extra strain at the interface. This design tradeoff between the enhancement in the thermal conductivity and reduction in the TBC by substrate offcut angle should be carefully balanced based on the application specifics. Finally, a remarkable reduction in the thermal conductivity caused by alloying should not be overlooked during device design phase of DUV optoelectronics and power electronics based on the β-Ga$_2$O$_3$.

EXPERIMENTAL METHODS

Metalorganic vapor phase epitaxy (MOVPE) growth of Ga$_2$O$_3$ and (Al$_x$Ga$_{1-x}$)$_2$O$_3$ thin films

MOVPE growth of UID β-phase Ga$_2$O$_3$ and (Al$_x$Ga$_{1-x}$)$_2$O$_3$ films was performed using an Agnitron Agilis MOVPE reactor with triethyl gallium (TEGa), trimethyl aluminum (TMAl), and O$_2$ as precursors. MOVPE growth of β-Ga$_2$O$_3$ and β-(Al$_x$Ga$_{1-x}$)$_2$O$_3$ films was performed on on-axis and 6° offcut (with respect to the a-plane) c-plane sapphire wafers. The substrates were first cleaned with acetone, isopropyl alcohol, and DI water before loading into the chamber. The growth temperature for all films was kept between 800°C – 880°C. The typical growth conditions used for the MOVPE growth are: TEGa 22 – 105 sccm, O$_2$ 250 – 800 sccm, and pressure 15 – 60 Torr. The growth time was varied between 30 mins – 2.5 hours to obtain films of the required thickness. Growth of β-(Al$_x$Ga$_{1-x}$)$_2$O$_3$ films was achieved by using a combination of TEGa and TMAl precursors. The Al composition was increased by increasing the [Al]/[Ga]+[Al] precursor molar ratio.

MOVPE-grown (010) β-Ga$_2$O$_3$ films with mobility close to the theoretical limit have been reported.[57] However, direct growth on other orientations ((100), ($\bar{2}$01), (001)) has led to films with lower mobility due to the higher density of structural defects.[58,59] It has been shown that high-quality (100)-oriented β-Ga$_2$O$_3$ thin films can be grown by choosing a β-Ga$_2$O$_3$ substrate with the correct offcut orientation, which suppresses the formation of structural defects.[60] Similar defects have been observed in MOVPE-grown ($\bar{2}$01) homoepitaxial β-Ga$_2$O$_3$ films.[58] Therefore, both low and high quality ($\bar{2}$01)-oriented heteroepitaxial β-Ga$_2$O$_3$ films were grown in this work using 0° and 6° off-angled c-plane sapphire substrates, respectively.

Low pressure chemical vapor deposition (LPCVD) growth of Ga$_2$O$_3$ thin films

Unintentionally-doped (UID) heteroepitaxial β-Ga$_2$O$_3$ films were grown on both on-axis and off-axis (6° towards <11$\bar{2}$0>) c-plane sapphire substrates in a custom-built LPCVD system. Details of setup for film deposition can be found in our previous work[28]. β-Ga$_2$O$_3$ thin films prepared in this paper were grown at a growth temperature of 900 °C and a chamber pressure of 2 Torr.

Typical LPCVD grown UID heteroepitaxial β-Ga$_2$O$_3$ films on sapphire substrates were found to be electrically insulating due to possible compensation effects. Si-doped films grown under similar growth conditions (900 °C) have shown controllable n-type doping with a wide doping range. Typical room temperature mobilities measured from LPCVD heteroepitaxial β-Ga$_2$O$_3$ thin films ranged between 40 ~ 60 cm^2/Vs when grown on on-axis c-plane sapphire, and 60 ~ 110 cm^2/Vs when grown on 6° off-cut sapphire, for a typical doping concentration of 10^{17}cm^{-3} ~ 10^{18} cm^{-3}.[23,28,29]

Scanning electron microscopy (SEM)

Scanning electron microscope (SEM) images of the surface of the β-Ga2O3 films were collected at varying magnifications to characterize the surface morphology and grain structure. Cross-sectional images were also obtained to measure the thicknesses of the films. The samples were cleaved to obtain these cross-sectional measurements of the fracture surface. For samples that were too small to physically cleave, a cross-section was prepared by focused ion beam (FIB) with an approximately 2 μm thick carbon cap. All SEM images were collected at 5 kV in a Mira TESCAN3 system with the exception for the FIB sections, which were prepared and imaged in a FEI Scios II system at a 52° tilt (accounted for during measurements).

To confirm the film thickness of the specimens, additional SEM images were collected on a Zeiss Supra55 VP at 20 kV with an aperture size of 120 mm in high current mode. The working distance for all images was 10 mm (±0.1 mm). Copper tape was used on samples to dissipate charge, but there was still noticeable charging in some regions which limited the spatial resolution. A backscattered electron detector was used for most imaging as it made phase and z contrast more prominent. Samples were cleaved and then mounted onto a cross-sectional stub for imaging.

X-ray diffraction (XRD)

X-ray diffraction (XRD) was used to confirm the phase and orientation, and to assess the crystalline quality of the films. First, 2-Theta (2Θ) scans were obtained using a Malvern Panalytical Empyrean system with Cu Kα_1=1.54 Å radiation in the Bragg-Brentano geometry. These scans were collected over a wide range (10-70° 2Θ) to verify the phase and identify the film and substrate peaks (when applicable). Within this range, ($\bar{2}$01)-oriented β-Ga$_2$O$_3$ is anticipated to exhibit diffraction peaks at 18.964°, 38.404°, and 59.236° 2Θ corresponding to the ($\bar{2}$01), ($\bar{4}$02), and ($\bar{6}$03) symmetric reflections, respectively (ICSD 04-008-8217). The (0006) peak of the c-plane Al$_2$O$_3$ substrate is also observed at 41.680° 2Θ (ICSD 01-074-1081). Next, high resolution scans were collected using a Malvern Materials Research Diffractometer (MRD) system in line focus mode with Cu Kα_1=1.54 Å radiation. This system is equipped with a five-axis goniometer, 2xGe (220) hybrid monochromator, and PIXcel detector with a fixed anti-scatter slit. All XRD characterization was completed at room temperature in this study.

The general procedure for collecting these scans begins by finding the coarse substrate offcut angle/tilt direction with a Laue diffractometer (for sample pieces without a flat). The sample is then loaded into the MRD system and fine calibration offsets were applied. For a c-plane Al$_2$O$_3$ substrate, the sample is initially aligned using the (0006) substrate peak. Then, a coupled ω-2Θ scan is obtained over a wide range of 10-70° 2Θ. From this scan, a film peak (e.g., ($\bar{2}$01)) is selected for an XRD rocking curve measurement. Before obtaining this measurement, the sample is aligned to the film peak by completing successive omega (ω) and chi (χ) scans over progressively narrow ranges to optimize the sample tilt by maximizing intensity. Additionally, X and Y line scans are completed to select the measurement location based on maximum intensity. Finally, to obtain the rocking curve, an ω scan was collected over a range of 6° with a 0.01° step size and dwell time of 0.1 s. In this study, rocking curves were obtained for both the ($\bar{2}$01) and ($\bar{4}$02) symmetric reflections. For the bulk β-Ga$_2$O$_3$ substrate a narrower range of 1.0° was utilized with a smaller step size of 0.001° to ensure a sufficient number of data points over the breadth of the peak. The full-width-at-half-maximum (FWHM) was calculated for each rocking curve, where a lower value implies superior crystalline quality.

Raman spectroscopy

β-Ga$_2$O$_3$ has 15 Raman-active phonon modes.[45] Among these, the A$_g$(3) phonon mode near 199.7 cm^{-1} was used in this study due to its relatively large intensity. The room temperature Raman spectra were obtained using a Horiba LabRAM HR Evolution spectrometer equipped with a 532 nm laser and a 1800 grooves/mm grating. A long working distance 50× objective (NA = 0.45) was used to probe the samples. Since the laser excitation energy (2.33 eV) is smaller than the bandgap energy of β-Ga$_2$O$_3$ (4.8 eV) and the sapphire substrate (8.8 eV), the laser heating was assumed to be negligible; therefore, a high laser power of ~20 mW was used. The results were based on five repeated measurements at three random locations on each sample. According to the energy-time uncertainty principle, as the crystalline quality decreases, the linewidth of the A$_g$(3) phonon mode will increase as a result of decreased phonon lifetime. Therefore, the linewidth was used to qualitatively compare the crystalline quality of the β-Ga$_2$O$_3$ samples.

Time-domain thermoreflectance (TDTR)

TDTR is an optical pump-probe technique that allows to measure the thermo-physical properties of thin films based on heat diffusion from ultrafast femtosecond laser pulses.[47] Details of the setup for TDTR measurements used in this study can be found in our previous work[54]. The radii of the focused pump and probe beams were characterized using a scanning-slit optical beam profiler (Thorlabs BP209-VIS) and were 7.0 μm and 4.5 μm, respectively. It should be noted that TDTR and FDTR measurements require a relatively smooth sample surface [31]; in this study, only samples with a reflected probe signal intensity

greater than 40% of that for a smooth Au/Si calibration sample were included, which is expected to have a RMS surface roughness less than 30 nm. Literature values were used for the thermal conductivity of Au as well as volumetric heat capacities (c_v) of Au[61], β-Ga$_2$O$_3$[62] and α-Al$_2$O$_3$[63] where the value of C_v for β-(Al$_x$Ga$_{1-x}$)$_2$O$_3$ was approximated as a weighted average of the constitutive materials based on the alloy composition. The temperature dependent thermal properties for the Au transducer[64], sapphire substrate[65], and β-Ga$_2$O$_3$[66] were taken from literature. The thermal boundary conductance (TBC) between the metal transducer and the β-Ga$_2$O$_3$ films was fitted simultaneously with the β-Ga$_2$O$_3$ thermal conductivity. Due to the exclusive high sensitivity (as shown in **Figure 12**), TDTR fits the β-Ga$_2$O$_3$ thermal conductivity accurately without being affected by the assumption for the TBC between the β-Ga$_2$O$_3$ films and the substrate. The uncertainty was calculated based on 95% confidence bounds from the random spots and ± 2 nm uncertainty associated with the transducer thickness.

Frequency-domain thermoreflectance (FDTR)

FDTR is an optical pump-probe technique that extracts the thermal properties of thin films from the phase response of a thermal wave over a range of modulation frequencies[48]. Details of the FDTR setup used in this study can be found in our previous work[54]. The radii of the focused pump and probe beams were 13.4 μm and 13.1 μm, respectively. Material properties used in the FDTR fitting model were identical to those used in the TDTR model. To extract the thermal boundary conductance of the MOVPE-grown samples, the thermal conductivities of the films were adopted from the TDTR measurement results to reduce the number of fitting parameters. The FDTR has a relatively low sensitivity to the TBC between the β-Ga$_2$O$_3$ films and the substrate (G2) as shown in **Figure 12**; therefore, a qualitative assessment of the TBCs were made based other parameters determined by TDTR. The upper and lower bounds of G2 were determined based on the 95% confidence bounds for the thermal conductivity of β-Ga$_2$O$_3$ films and the substrates. Representative fitting for TDTR and FDTR is shown in **Figure 13**.
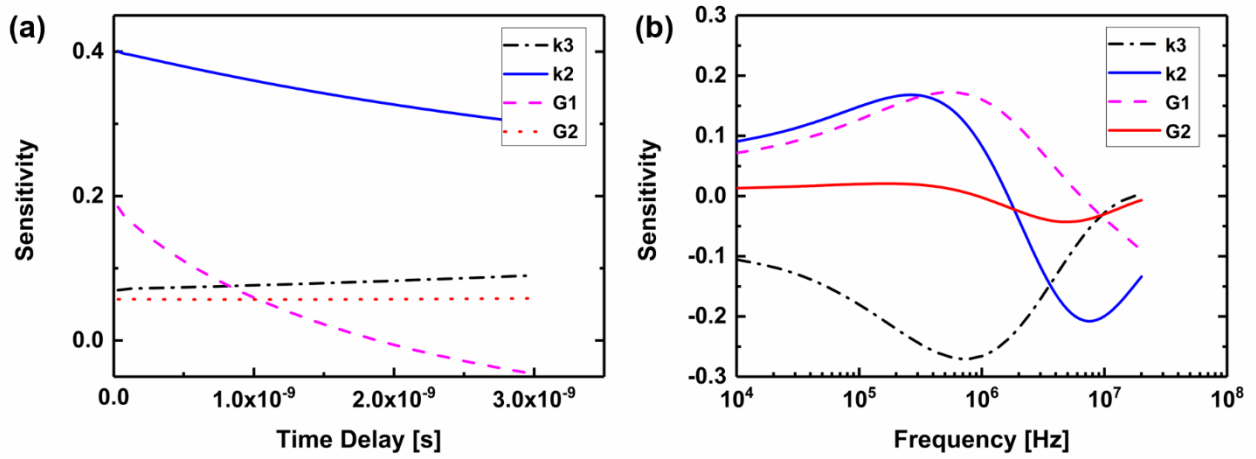
Figure 12. The sensitivity plot for 164 nm thick MOVPE-grown β-Ga$_2$O$_3$ film on c-plane sapphire measured by a) TDTR, and b) FDTR. In the legend, k2 is the cross-plane thermal conductivity of the β-Ga$_2$O$_3$ film. k3 is the thermal conductivity of the sapphire substrate. G1 and G2 are the thermal boundary conductance of the transducer- β-Ga$_2$O$_3$ and β-Ga$_2$O$_3$-substrate interfaces, respectively.

15
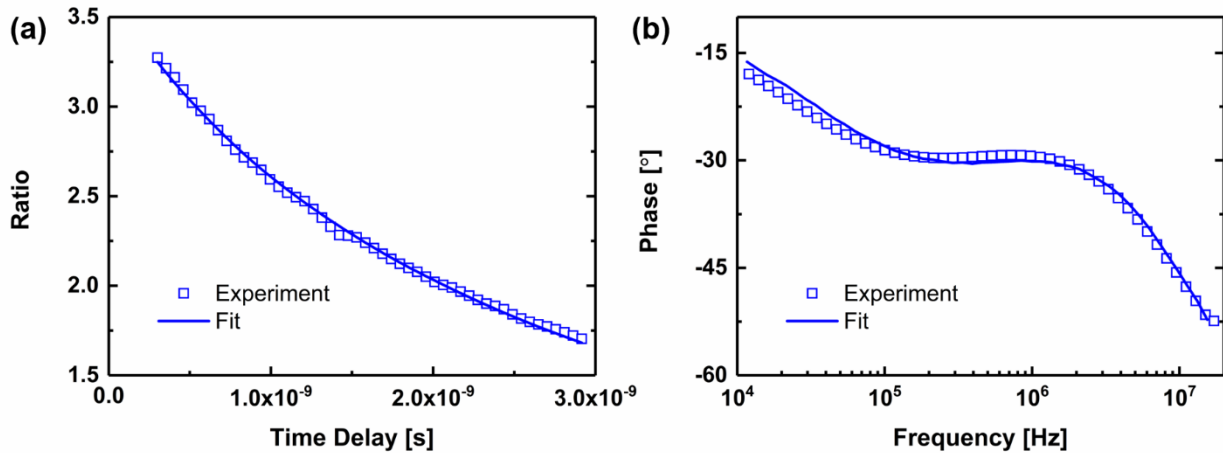
Figure 13. The data fitting for 164 nm thick MOVPE-grown β-Ga$_2$O$_3$ film on c-plane sapphire measured by a) TDTR, and b) FDTR.

Scanning transmission electron microscopy (STEM)

Cross-sectional TEM samples were prepared using focused ion beam. To identify the crystalline quality at the atomic scale in the interface regions, thin and clean TEM foils were obtained using a low-energy (500 eV) ion milling (Fischione Nanomill). High-resolution STEM high angle annular dark filed (HAADF) imaging was performed using a probe corrected Thermo Fisher Scientific Themis Z STEM mode (Cs$_3$=0.002 mm, Cs$_5$=1.0 mm) with probe convergence half angles of 17.9 mrad at an accelerating voltage of 200 kV. Since HAADF-STEM image contrast is approximately proportional to the square of atomic number, contrast patterns resulted from the different crystal structures of the Ga$_2$O$_3$ and the Al$_2$O$_3$ were atomically differentiated.

THEORETICAL CALCULATIONS

First principles calculations

First-principles calculations of the phonon structure as well as the anharmonic phonon coupling were performed with the ShengBTE software package[67]. Density Functional Theory (DFT) total energy calculations were utilized for the computation of interatomic force constants (IFCs) using the QuantumEspresso package[68]. For anharmonic as well as harmonic force constants, single atoms were displaced in a supercell for various configurations based on the symmetry of the crystal. Total energy calculations from the various displaced supercells allow forces, and subsequently IFCs, to be computed. In this work, a 2×2×2 supercell containing 80 atoms was utilized with a 2×2×2 k-point sampling grid for subsequent self-consistent total energy calculations in computing the force-constant matrix as well as the phonon-phonon coupling matrix elements. These phonon-phonon coupling matrix elements were used to determine the scattering rates necessary for a single-mode relaxation time approximation of the phonon Boltzmann transport equation. Full details of the Boltzmann transport equation solution for thermal conductivity can be found in reference [30].

Thermal conductivity modeling

The Debye-Callaway model was applied to obtain the thickness-dependent thermal conductivity of β-Ga$_2$O$_3$ single crystals along the ⊥ ($\bar{2}$01) direction.[11] The phonon-phonon Umklapp scattering, phonon-impurity scattering, and phonon-boundary scattering are included in the resistive phonon scattering processes of the model. The scattering rates of the three scattering mechanisms are expressed as

$$\left[\tau_U^j(x)\right]^{-1} = \frac{k_{\mathrm{B}}^2 \gamma_j^2}{M\hbar v_j^2 \theta_j} x^2 T^3 e^{-\frac{\theta_j}{3T}} \tag{1}$$

$$\left[\tau_I^j(x)\right]^{-1} = \frac{V k_{\mathrm{B}}^4 \Gamma}{4\pi \hbar^4 v_j^3} x^4 T^4 \tag{2}$$

$$\left[\tau_B^j\right]^{-1} = \frac{v_j}{d} \tag{3}$$

where k_{B} is the Boltzmann constant, T is the temperature, $\hbar$ is the reduced Planck's constant, θ is the Debye temperature, v is the phonon velocity, subscript "j" denotes the branch in the phonon dispersion spectrum, and $x = \hbar\omega/k_{\mathrm{B}}T$ with ω being the angular frequency. For β-Ga$_2$O$_3$, $V = 1.0587 \times 10^{-29}$ m^3/atom and $M = 6.2231 \times 10^{-26}$ kg/atom. The Grüneisen parameters, γ_{L} and γ_{T}, are treated as two fitting parameters and are obtained by fitting the temperature-dependent thermal conductivity from 100 to 700 K to the first-principles calculations along the ⊥ ($\bar{2}$01) direction of bulk β-Ga$_2$O$_3$. The parameters that were used in the model calculation are listed in **Table 1**. These parameters were derived from the aforementioned first principles calculations, which are in good agreement with values reported in literature[10]. Parameters associated with other crystallographic directions of β-Ga$_2$O$_3$ can be found in open literature[10,37].

Table 1. Zone-boundary frequencies $f_{L,T}$ and phonon velocities $v_{L,T}$ of longitudinal and transverse phonons for β-Ga$_2$O$_3$ along the ⊥ ($\bar{2}$01) direction from the first-principles calculations. $\theta_{L,T}$ are the Debye temperatures calculated from these cutoff frequencies following $\theta = \frac{2\pi\hbar f}{k_B}$. $\gamma_{L,T}$ are the Grüneisen parameters.

Direction	f_L (THz)	f_{T1} (THz)	f_{T2} (THz)	v_L (m s^{-1})	v_{T1} (m s^{-1})	v_{T2} (m s^{-1})	θ_L (K)	θ_{T1} (K)	θ_{T2} (K)	γ_L	γ_T

16

⊥ ($\bar{2}01$)	3.9	2.5	2.3	6656	3206	2385	187	120	110	1.1	0.78

AMM and DMM

The TBC for the β-Ga$_2$O$_3$/sapphire interface was analytically calculated by implementing the Landauer formalism with the acoustic mismatch (AMM) and diffusive mismatch (DMM) models. The general Landauer formula for the TBC can be expressed as follows:

$$G = \sum_p \frac{1}{2} \int_0^{\omega_d} \int_0^{\pi/2} D_1(\omega) \frac{df_{BE}}{dT} \hbar \omega v_1(\omega) \tau_{1,2}(\theta, \omega) \cos(\theta) \sin(\theta) \, d\theta d\omega \quad (4)$$

where D represents the phonon density of states (DOS), f_{BE} is the Bose-Einstein distribution function of phonons, $\hbar$ is the reduced Planck constant, ω represents the angular frequency, ω_d represents the cutoff frequency, v is the phonon group, $\tau_{1,2}$ is the transmission coefficient from the medium 1 to 2, θ is the angle of incidence, and the index p indicates the phonon branch. For the AMM, the transmission coefficient can be expressed as

$$\tau_{1,2,\text{AMM}}(\theta, \omega) = \frac{4 \frac{Z_2}{Z_1} \cdot \frac{\cos(\theta_2)}{\cos(\theta_1)}}{\left(\frac{Z_2}{Z_1} + \frac{\cos(\theta_2)}{\cos(\theta_1)}\right)^2} \quad (5)$$

Alternatively, since the transmission function for DMM does not depend on the angle of incidence, the integration over θ is not needed, and the transmission coefficient adopts the following form

$$\tau_{1,2,\text{DMM}}(\omega) = \frac{\sum_p M_2(\omega)}{\sum_p M_1(\omega) + \sum_p M_2(\omega)} \quad (6)$$

where Z is the acoustic impedance and M is the phonon number of modes of mediums 1 and 2. The formulations of the AMM and DMM presented by Bellis et al. [49] were adopted in the present study, and the model input parameters are listed in Table 2.

Table 2. Parameters implemented for the calculations of the thermal boundary conductance (G) using the AMM and DMM formulations.

Medium A	Medium B	Speed of sound [m/s] v_L, v_T		Mass density [kg/m^3]		G_{AMM}	G_{DMM}
		Medium A	Medium B	Medium A	Medium B	[MWm^{-2}K^{-1}]	[MWm^{-2}K^{-1}]
β-Ga$_2$O$_3$ [$\bar{2}01$]	Sapphire c-plane	6600, 2750[10]	11260, 6467[69,70]	5880	3980	522.8069	72.65426

AUTHOR INFORMATION

Corresponding Author
* E-mail: sukwon.choi@psu.edu

ACKNOWLEDGMENT

REFERENCES

(1) Wei, T.; Tsai, D.; Ravadgar, P.; Ke, J.; Tsai, M.; Lien, D.; Huang, C.; Horng, R.; He, J. See-Through Ga2O3 Solar-Blind Photodetectors for Use in Harsh Environments. *IEEE J. Sel. Top. Quantum Electron.* **2014**, *20* (6), 112–117. https://doi.org/10.1109/JSTQE.2014.2321517.

(2) Higashiwaki, M.; Jessen, G. H. Guest Editorial: The Dawn of Gallium Oxide Microelectronics. *Appl. Phys. Lett.* **2018**, *112* (6), 60401. https://doi.org/10.1063/1.5017845.

(3) Pearton, S. J.; Yang, J.; Cary, P. H.; Ren, F.; Kim, J.; Tadjer, M. J.; Mastro, M. A. A Review of Ga2O3 Materials, Processing, and Devices. *Appl. Phys. Rev.* **2018**, *5* (1), 11301. https://doi.org/10.1063/1.5006941.

(4) Rafique, S.; Han, L.; Zhao, H. Thermal Annealing Effect on β-Ga2O3 Thin Film Solar Blind Photodetector Heteroepitaxially Grown on Sapphire Substrate. *Phys. status solidi* **2017**, *214* (8), 1700063. https://doi.org/10.1002/pssa.201700063.

(5) Krishnamoorthy, S.; Xia, Z.; Joishi, C.; Zhang, Y.; McGlone, J.; Johnson, J.; Brenner, M.; Arehart, A. R.; Hwang, J.; Lodha, S.; Rajan, S. Modulation-Doped β-(Al0.2Ga0.8)2O3/Ga2O3 Field-Effect Transistor. *Appl. Phys. Lett.* **2017**, *111* (2), 23502. https://doi.org/10.1063/1.4993569.

(6) Chatterjee, B.; Song, Y.; Lundh, J. S. J. S.; Zhang, Y.; Xia, Z.; Islam, Z.; Leach, J.; McGray, C.; Ranga, P.; Krishnamoorthy, S.; Haque, A.; Rajan, S.; Choi, S. Electro-Thermal Co-Design of β-(AlxGa1-x)2O3/Ga2O3 Modulation Doped Field Effect Transistors. *Appl. Phys. Lett.* **2020**, *117* (15), 153501. https://doi.org/10.1063/5.0021275.

(7) Chatterjee, B.; Zeng, K.; Nordquist, C. D.; Singisetti, U.; Choi, S. Device-Level Thermal Management of Gallium Oxide Field-Effect Transistors. *IEEE Trans. Components, Packag. Manuf. Technol.* **2019**, *9* (12), 2352–2365. https://doi.org/10.1109/tcpmt.2019.2923356.

(8) Chatterjee, B.; Jayawardena, A.; Heller, E.; Snyder, D. W.; Dhar, S.; Choi, S. Thermal Characterization of Gallium Oxide Schottky Barrier Diodes. *Rev. Sci. Instrum.* **2018**, *89* (11), 114903. https://doi.org/10.1063/1.5053621.

(9) Lundh, J. S.; Zhang, T.; Zhang, Y.; Xia, Z.; Wetherington, M.; Lei, Y.; Kahn, E.; Rajan, S.; Terrones, M.; Choi, S. 2D Materials for Universal Thermal Imaging of Micro- and Nanodevices: An Application to Gallium Oxide Electronics. *ACS Appl. Electron. Mater.* **2020**, *2* (9). https://doi.org/10.1021/acsaelm.0c00574.

(10) Guo, Z.; Verma, A.; Wu, X.; Sun, F.; Hickman, A.; Masui, T.; Kuramata, A.; Higashiwaki, M.; Jena, D.; Luo, T. Anisotropic Thermal Conductivity in Single Crystal β-Gallium Oxide. *Appl. Phys. Lett.* **2015**, *106* (11), 1–6. https://doi.org/10.1063/1.4916078.

(11) Jiang, P.; Qian, X.; Li, X.; Yang, R. Three-Dimensional Anisotropic Thermal Conductivity Tensor of Single Crystalline β-Ga2O3. *Appl. Phys. Lett.* **2018**, *113* (23), 232105. https://doi.org/10.1063/1.5054573.

(12) Alema, F.; Hertog, B.; Osinsky, A.; Mukhopadhyay, P.; Toporkov, M.; Schoenfeld, W. V. Fast Growth Rate of Epitaxial β–Ga2O3 by Close Coupled Showerhead MOCVD. *J. Cryst. Growth* **2017**, *475*, 77–82. https://doi.org/https://doi.org/10.1016/j.jcrysgro.2017.06.001.

(13) Bhattacharyya, A.; Ranga, P.; Roy, S.; Ogle, J.; Whittaker-Brooks, L.; Krishnamoorthy, S. Low Temperature Homoepitaxy of (010) -Ga2O3by Metalorganic Vapor Phase Epitaxy: Expanding the Growth Window. *Appl. Phys. Lett.* **2020**, *117* (14). https://doi.org/10.1063/5.0023778.

(14) Ghadi, H.; McGlone, J. F.; Jackson, C. M.; Farzana, E.; Feng, Z.; Bhuiyan, A. F. M. A. U.; Zhao, H.; Arehart, A. R.; Ringel, S. A. Full Bandgap Defect State Characterization of β-Ga2O3 Grown by Metal Organic Chemical Vapor Deposition. *APL Mater.* **2020**, *8* (2), 21111. https://doi.org/10.1063/1.5142313.

(15) Feng, Z.; Anhar Uddin Bhuiyan, A. F. M. M.; Karim, M. R.; Zhao, H. MOCVD Homoepitaxy of Si-Doped (010) β-Ga2O3 Thin Films with Superior Transport Properties. *Appl. Phys. Lett.* **2019**, *114* (25), 250601. https://doi.org/10.1063/1.5109678.

(16) Alema, F.; Zhang, Y.; Osinsky, A.; Orishchin, N.; Valente, N.; Mauze, A.; Speck, J. S. Low 1014 Cm−3 Free Carrier Concentration in Epitaxial β-Ga2O3 Grown by MOCVD. *APL Mater.* **2020**, *8* (2), 21110. https://doi.org/10.1063/1.5132752.

(17) Seryogin, G.; Alema, F.; Valente, N.; Fu, H.; Steinbrunner, E.; Neal, A. T.; Mou, S.; Fine, A.; Osinsky, A. MOCVD Growth of High Purity Ga2O3 Epitaxial Films Using Trimethylgallium Precursor. *Appl. Phys. Lett.* **2020**, *117* (26), 262101. https://doi.org/10.1063/5.0031484.

(18) Anhar Uddin Bhuiyan, A. F. M.; Feng, Z.; Johnson, J. M.; Chen, Z.; Huang, H. L.; Hwang, J.; Zhao, H. MOCVD Epitaxy of β -(AlxGa1-x)2O3 Thin Films on (010) Ga2O3 Substrates and N-Type Doping. *Appl. Phys. Lett.* **2019**, *115* (12), 1–6. https://doi.org/10.1063/1.5123495.

(19) Ranga, P.; Rishinaramangalam, A.; Varley, J.; Bhattacharyya, A.; Feezell, D.; Krishnamoorthy, S. Si-Doped β-(Al0.26Ga0.74)2O3 Thin Films and Heterostructures Grown by Metalorganic Vapor-Phase Epitaxy. *Appl. Phys. Express* **2019**, *12* (11), 111004. https://doi.org/10.7567/1882-0786/ab47b8.

(20) Bhuiyan, A. F. M. A. U.; Feng, Z.; Johnson, J. M.; Huang, H.-L.; Sarker, J.; Zhu, M.; Karim, M. R.; Mazumder, B.; Hwang, J.; Zhao, H. Phase Transformation in MOCVD Growth of (AlxGa1−x)2O3 Thin Films. *APL Mater.* **2020**, *8* (3), 31104. https://doi.org/10.1063/1.5140345.

(21) Bhuiyan, A. F. M. A. U.; Feng, Z.; Johnson, J. M.; Huang, H.-L.; Hwang, J.; Zhao, H. MOCVD Growth of β-Phase (AlxGa1−x)2O3 on (2̄01) β-

Ga2O3 Substrates. *Appl. Phys. Lett.* **2020**, *117* (14), 142107. https://doi.org/10.1063/5.0025478.

(22) Bhuiyan, A. F. M. A. U.; Feng, Z.; Johnson, J. M.; Huang, H.-L.; Hwang, J.; Zhao, H. Band Offsets of (100) β-(AlxGa1−x)2O3/β-Ga2O3 Heterointerfaces Grown via MOCVD. *Appl. Phys. Lett.* **2020**, *117* (25), 252105. https://doi.org/10.1063/5.0031584.

(23) Rafique, S.; Han, L.; Neal, A. T.; Mou, S.; Boeckl, J.; Zhao, H. Towards High-Mobility Heteroepitaxial β-Ga2O3 on Sapphire − Dependence on The Substrate Off-Axis Angle. *Phys. status solidi* **2018**, *215* (2), 1700467. https://doi.org/10.1002/pssa.201700467.

(24) Rafique, S.; Han, L.; Neal, A. T.; Mou, S.; Tadjer, M. J.; French, R. H.; Zhao, H. Heteroepitaxy of N-Type β-Ga2O3 Thin Films on Sapphire Substrate by Low Pressure Chemical Vapor Deposition. *Appl. Phys. Lett.* **2016**, *109* (13). https://doi.org/10.1063/1.4963820.

(25) Rafique, S.; Karim, M. R.; Johnson, J. M.; Hwang, J.; Zhao, H. LPCVD Homoepitaxy of Si Doped β-Ga2O3 Thin Films on (010) and (001) Substrates. *Appl. Phys. Lett.* **2018**, *112* (5), 52104. https://doi.org/10.1063/1.5017616.

(26) Rafique, S.; Han, L.; Tadjer, M. J.; Freitas, J. A.; Mahadik, N. A.; Zhao, H. Homoepitaxial Growth of β-Ga2O3 Thin Films by Low Pressure Chemical Vapor Deposition. *Appl. Phys. Lett.* **2016**, *108* (18), 182105. https://doi.org/10.1063/1.4948944.

(27) Rafique, S.; Han, L.; Zhao, H. Synthesis of Wide Bandgap Ga2O3 (Eg ~ 4.6–4.7 EV) Thin Films on Sapphire by Low Pressure Chemical Vapor Deposition. *Phys. status solidi* **2016**, *213* (4), 1002–1009. https://doi.org/10.1002/pssa.201532711.

(28) Feng, Z.; Karim, M. R.; Zhao, H. Low Pressure Chemical Vapor Deposition of β-Ga2O3 Thin Films: Dependence on Growth Parameters. *APL Mater.* **2018**, *7* (2), 22514. https://doi.org/10.1063/1.5054713.

(29) Zhang, Y.; Feng, Z.; Karim, M. R.; Zhao, H. High-Temperature Low-Pressure Chemical Vapor Deposition of β-Ga2O3. *J. Vac. Sci. Technol. A* **2020**, *38* (5), 50806. https://doi.org/10.1116/6.0000360.

(30) Santia, M. D.; Tandon, N.; Albrecht, J. D. Lattice Thermal Conductivity in β-Ga2O3 from First Principles. *Appl. Phys. Lett.* **2015**, *107* (4), 41907. https://doi.org/10.1063/1.4927742.

(31) Cahill, D. G.; Braun, P. V.; Chen, G.; Clarke, D. R.; Fan, S.; Goodson, K. E.; Keblinski, P.; King, W. P.; Mahan, G. D.; Majumdar, A.; Maris, H. J.; Phillpot, S. R.; Pop, E.; Shi, L. Nanoscale Thermal Transport. II. 2003-2012. *Appl. Phys. Rev.* **2014**, *1* (1). https://doi.org/10.1063/1.4832615.

(32) Cahill, D. G.; Ford, W. K.; Goodson, K. E.; Mahan, G. D.; Majumdar, A.; Maris, H. J.; Merlin, R.; Phillpot, S. R. Nanoscale Thermal Transport. *J. Appl. Phys.* **2003**, *93* (2), 793–818. https://doi.org/10.1063/1.1524305.

(33) Yan, Z.; Kumar, S. Phonon Mode Contributions to Thermal Conductivity of Pristine and Defective β-Ga2O3. *Phys. Chem. Chem. Phys.* **2018**, *20* (46), 29236–29242. https://doi.org/10.1039/C8CP05139A.

(34) Szwejkowski, C. J.; Creange, N. C.; Sun, K.; Giri, A.; Donovan, B. F.; Constantin, C.; Hopkins, P. E. Size Effects in the Thermal Conductivity of Gallium Oxide (β-Ga2O3) Films Grown via Open-Atmosphere Annealing of Gallium Nitride. *J. Appl. Phys.* **2015**, *117* (8). https://doi.org/10.1063/1.4913601.

(35) Cheng, Z.; Wheeler, V. D.; Bai, T.; Shi, J.; Tadjer, M. J.; Feygelson, T.; Hobart, K. D.; Goorsky, M. S.; Graham, S. Integration of Polycrystalline Ga2O3 on Diamond for Thermal Management. *Appl. Phys. Lett.* **2020**, *116* (6), 62105. https://doi.org/10.1063/1.5125637.

(36) Zhang, Y.; Su, Q.; Zhu, J.; Koirala, S.; Koester, S. J.; Wang, X. Thickness-Dependent Thermal Conductivity of Mechanically Exfoliated β-Ga2O3 Thin Films. *Appl. Phys. Lett.* **2020**, *116* (20), 202101. https://doi.org/10.1063/5.0004984.

(37) Cheng, Z.; Yates, L.; Shi, J.; Tadjer, M. J.; Hobart, K. D.; Graham, S. Thermal Conductance across β-Ga2O3-Diamond van Der Waals Heterogeneous Interfaces. *APL Mater.* **2019**, *7* (3). https://doi.org/10.1063/1.5089559.

(38) Cheng, Z.; Mu, F.; You, T.; Xu, W.; Shi, J.; Liao, M. E.; Wang, Y.; Huynh, K.; Suga, T.; Goorsky, M. S.; Ou, X.; Graham, S. Thermal Transport across Ion-Cut Monocrystalline β-Ga2O3 Thin Films and Bonded β-Ga2O3–SiC Interfaces. *ACS Appl. Mater. Interfaces* **2020**, *12* (40), 44943–44951. https://doi.org/10.1021/acsami.0c11672.

(39) Blumenschein, N.; Slomski, M.; Paskov, P. P.; Kaess, F.; Breckenridge, M. H.; Muth, J. F.; Paskova, T. Thermal Conductivity of Bulk and Thin Film β-Ga2O3 Measured by the 3ω Technique. In *Proc.SPIE*; 2018; Vol. 10533.

(40) Ambacher, O.; Smart, J.; Shealy, J. R.; Weimann, N. G.; Chu, K.; Murphy, M.; Schaff, W. J.; Eastman, L. F.; Dimitrov, R.; Wittmer, L.; Stutzmann, M.; Rieger, W.; Hilsenbeck, J. Two-Dimensional Electron Gases Induced by Spontaneous and Piezoelectric Polarization Charges in N- and Ga-Face AlGaN/GaN Heterostructures. *J. Appl. Phys.* **1999**, *85* (6), 3222. https://doi.org/10.1063/1.369664.

(41) Zhang, Y.; Xia, Z.; Mcglone, J.; Sun, W.; Joishi, C.; Arehart, A. R.; Ringel, S. A.; Rajan, S. Evaluation of Low-Temperature Saturation Velocity in β-(AlxGa1–x)2O3/Ga2O3 Modulation-Doped Field-Effect Transistors. *IEEE Trans. Electron Devices* **2019**, *66* (3), 1574–1578. https://doi.org/10.1109/TED.2018.2889573.

(42) Oshima, Y.; Víllora, E. G.; Shimamura, K. Quasi-Heteroepitaxial Growth of β-Ga2O3 on off-Angled Sapphire (0001) Substrates by Halide Vapor Phase Epitaxy. *J. Cryst. Growth* **2015**, *410*, 53–58. https://doi.org/https://doi.org/10.1016/j.jcrysgro.2014.10.038.

(43) Zhong, C.-T.; Zhang, G.-Y. Growth of N-Polar GaN on Vicinal Sapphire Substrate by Metal Organic Chemical Vapor Deposition. *Rare Met.* **2014**, *33* (6), 709–713. https://doi.org/10.1007/s12598-013-0163-5.

(44) Shen, X. Q.; Matsuhata, H.; Okumura, H. Reduction of the Threading Dislocation Density in GaN Films Grown on Vicinal Sapphire (0001) Substrates. *Appl. Phys. Lett.* **2005**, *86* (2), 21912. https://doi.org/10.1063/1.1849836.

(45) Kranert, C.; Sturm, C.; Schmidt-Grund, R.; Grundmann, M. Raman Tensor Elements of β-Ga2O3. *Sci. Rep.* **2016**, *6* (1), 35964. https://doi.org/10.1038/srep35964.

(46) Kuball, M. Raman Spectroscopy of GaN, AlGaN and AlN for Process and Growth Monitoring/Control. *Surf. Interface Anal.* **2001**, *31* (10), 987–999. https://doi.org/10.1002/sia.1134.

(47) Cahill, D. G. Analysis of Heat Flow in Layered Structures for Time-Domain Thermoreflectance. *Rev. Sci. Instrum.* **2004**, *75* (12), 5119–5122. https://doi.org/10.1063/1.1819431.

(48) Schmidt, A. J.; Cheaito, R.; Chiesa, M. A Frequency-Domain Thermoreflectance Method for the Characterization of Thermal Properties. *Rev. Sci. Instrum.* **2009**, *80* (9), 94901. https://doi.org/10.1063/1.3212673.

(49) De Bellis, L.; Phelan, P. E.; Prasher, R. S. Variations of Acoustic and Diffuse Mismatch Models in Predicting Thermal-Boundary Resistance. *J. Thermophys. Heat Transf.* **2000**, *14* (2), 144–150. https://doi.org/10.2514/2.6525.

(50) Adachi, S. Lattice Thermal Conductivity of Group-IV and III–V Semiconductor Alloys. *J. Appl. Phys.* **2007**, *102* (6), 63502. https://doi.org/10.1063/1.2779259.

(51) Chatterjee, B.; Lundh, J. S.; Song, Y.; Shoemaker, D.; Baca, A. G.; Kaplar, R. J.; Beechem, T. E.; Saltonstall, C.; Allerman, A. A.; Armstrong, A. M.; Klein, B. A.; Bansal, A.; Seyf, H. R.; Talreja, D.; Pogrebnyakov, A.; Heller, E.; Gopalan, V.; Henry, A. S.; Redwing, J. M.; Foley, B.; Choi, S. Interdependence of Electronic and Thermal Transport in AlxGa1-XN Channel HEMTs. *IEEE Electron Device Lett.* **2020**, 1. https://doi.org/10.1109/LED.2020.2969515.

(52) He, Y.; Donadio, D.; Galli, G. Heat Transport in Amorphous Silicon: Interplay between Morphology and Disorder. *Appl. Phys. Lett.* **2011**, *98* (14), 144101. https://doi.org/10.1063/1.3574366.

(53) Cheng, Z.; Tanen, N.; Chang, C.; Shi, J.; McCandless, J.; Muller, D.; Jena, D.; Xing, H. G.; Graham, S. Significantly Reduced Thermal Conductivity in β-(Al0.1Ga0.9)2O3/Ga2O3 Superlattices. *Appl. Phys. Lett.* **2019**, *115* (9), 92105. https://doi.org/10.1063/1.5108757.

(54) Song, Y.; Perez, C.; Esteves, G.; Lundh, J. S.; Saltonstall, C. B.; Beechem, T. E.; Yang, J. I.; Ferri, K.; Brown, J. E.; Tang, Z.; Maria, J.-P.; Snyder, D. W.; Olsson, R. H.; Griffin, B. A.; Trolier-McKinstry, S. E.; Foley, B. M.; Choi, S. Thermal Conductivity of Aluminum Scandium Nitride for 5G

Mobile Applications and Beyond. *ACS Appl. Mater. Interfaces* **2021**. https://doi.org/10.1021/acsami.1c02912.

(55) Tarumi, R.; Ledbetter, H.; Ogi, H.; Hirao, M. Low-Temperature Elastic Constants of Monocrystal Corundum (α-Al2O3). *Philos. Mag.* **2013**, *93* (36), 4532–4543. https://doi.org/10.1080/14786435.2013.837225.

(56) He, H.; Blanco, M. A.; Pandey, R. Electronic and Thermodynamic Properties of β-Ga2O3. *Appl. Phys. Lett.* **2006**, *88* (26), 261904. https://doi.org/10.1063/1.2218046.

(57) Bhattacharyya, A.; Ranga, P.; Roy, S.; Krishnamoorthy, S. High-Density Electron Gas β-Ga2O3 Field Effect Transistors with Metalorganic Vapor Phase Epitaxy-Regrown Ohmic Contacts. In *Device Research Conference*; 2020.

(58) Eisner, B. A.; Ranga, P.; Bhattacharyya, A.; Krishnamoorthy, S.; Scarpulla, M. A. Compensation in (2‾01) Homoepitaxial β-Ga2O3 Thin Films Grown by Metalorganic Vapor-Phase Epitaxy. *J. Appl. Phys.* **2020**, *128* (19), 195703. https://doi.org/10.1063/5.0022043.

(59) Fiedler, A.; Schewski, R.; Baldini, M.; Galazka, Z.; Wagner, G.; Albrecht, M.; Irmscher, K. Influence of Incoherent Twin Boundaries on the Electrical Properties of β-Ga2O3 Layers Homoepitaxially Grown by Metal-Organic Vapor Phase Epitaxy. *J. Appl. Phys.* **2017**, *122* (16), 165701. https://doi.org/10.1063/1.4993748.

(60) Schewski, R.; Lion, K.; Fiedler, A.; Wouters, C.; Popp, A.; Levchenko, S. V; Schulz, T.; Schmidbauer, M.; Bin Anooz, S.; Grüneberg, R.; Galazka, Z.; Wagner, G.; Irmscher, K.; Scheffler, M.; Draxl, C.; Albrecht, M. Step-Flow Growth in Homoepitaxy of β-Ga2O3 (100)—The Influence of the Miscut Direction and Faceting. *APL Mater.* **2018**, *7* (2), 22515. https://doi.org/10.1063/1.5054943.

(61) Touloukian, Y. S.; Buyco, E. H. *Thermophysical Properties of Matter - the TPRC Data Series. Volume 4. Specific Heat - Metallic Elements and Alloys. (Reannouncement). Data Book*; United States, 1971.

(62) Adams, G. B.; Johnston, H. L. Low Temperature Heat Capacities of Inorganic Solids. XI. The Heat Capacity of β-Gallium Oxide from 15 to 300°K.1. *J. Am. Chem. Soc.* **1952**, *74* (19), 4788–4789. https://doi.org/10.1021/ja01139a018.

(63) Ditmars, D. A.; Ishihara, S.; Chang, S. S.; Bernstein, G.; West, E. D. Enthalpy and Heat-Capacity Standard Reference Material: Synthetic Sapphire (Alpha -Al2O3) from 10 to 2250 K. *J. Res. Natl. Bur. Stand. (United States)* **1982**, *87* (2), 159–163. https://doi.org/10.6028/jres.087.012.

(64) Arblaster, J. W. Thermodynamic Properties of Gold. *J. Phase Equilibria Diffus.* **2016**, *37* (2), 229–245. https://doi.org/10.1007/s11669-016-0449-z.

(65) Schulz, B. High Temperature Thermal Conductivity of Irradiated and Non-Irradiated α-Al2O3. *J. Nucl. Mater.* **1988**, *155–157*, 348–351. https://doi.org/https://doi.org/10.1016/0022-3115(88)90269-3.

(66) Yoshioka, S.; Hayashi, H.; Kuwabara, A.; Oba, F.; Matsunaga, K.; Tanaka, I. Structures and Energetics of Ga2O3 Polymorphs. *J. Phys. Condens. Matter* **2007**, *19* (34). https://doi.org/10.1088/0953-8984/19/34/346211.

(67) Li, W.; Carrete, J.; A. Katcho, N.; Mingo, N. ShengBTE: A Solver of the Boltzmann Transport Equation for Phonons. *Comput. Phys. Commun.* **2014**, *185* (6), 1747–1758. https://doi.org/https://doi.org/10.1016/j.cpc.2014.02.015.

(68) Giannozzi, P.; Baroni, S.; Bonini, N.; Calandra, M.; Car, R.; Cavazzoni, C.; Ceresoli, D.; Chiarotti, G. L.; Cococcioni, M.; Dabo, I.; Dal Corso, A.; de Gironcoli, S.; Fabris, S.; Fratesi, G.; Gebauer, R.; Gerstmann, U.; Gougoussis, C.; Kokalj, A.; Lazzeri, M.; Martin-Samos, L.; Marzari, N.; Mauri, F.; Mazzarello, R.; Paolini, S.; Pasquarello, A.; Paulatto, L.; Sbraccia, C.; Scandolo, S.; Sclauzero, G.; Seitsonen, A. P.; Smogunov, A.; Umari, P.; Wentzcovitch, R. M. QUANTUM ESPRESSO: A Modular and Open-Source Software Project for Quantum Simulations of Materials. *J. Phys. Condens. Matter* **2009**, *21* (39), 395502. https://doi.org/10.1088/0953-8984/21/39/395502.

(69) Winey, J. M.; Gupta, Y. M.; Hare, D. E. R-Axis Sound Speed and Elastic Properties of Sapphire Single Crystals. *J. Appl. Phys.* **2001**, *90* (6), 3109–3111. https://doi.org/10.1063/1.1391420.

(70) Pedrós, J.; Calle, F.; Grajal, J.; Jiménez Riobóo, R. J.; Takagaki, Y.; Ploog, K. H.; Bougrioua, Z. Anisotropy-Induced Polarization Mixture of Surface Acoustic Waves in GaN∕c-Sapphire Heterostructures. *Phys. Rev. B* **2005**, *72* (7), 75306. https://doi.org/10.1103/PhysRevB.72.075306.